

# On the Sensitivity of Partial Redistribution Scattering Polarization Profiles to Various Atmospheric Parameters

M. Sampoorna<sup>1,†</sup>, J. Trujillo Bueno<sup>1,2,3</sup>, and E. Landi Degl’Innocenti<sup>1,4</sup>

<sup>1</sup>*Instituto de Astrofísica de Canarias, E-38205 La Laguna, Tenerife, Spain*

<sup>2</sup>*Departamento de Astrofísica, Facultad de Física, Universidad de La Laguna, Tenerife, Spain*

<sup>3</sup>*Consejo Superior de Investigaciones Científicas, Spain*

<sup>4</sup>*Dipartimento di Fisica e Astronomia, Sezione di Astronomia e Scienza dello Spazio, Università degli Studi di Firenze, Largo Enrico Fermi 2, I-50125 Firenze, Italy*

sampoorna@iiap.res.in; jtb@iac.es; landie@arcetri.astro.it

Accepted in August 2010 for publication in *The Astrophysical Journal*

## ABSTRACT

This paper presents a detailed study of the scattering polarization profiles formed under partial frequency redistribution (PRD) in two thermal models of the solar atmosphere. Particular attention is given to understanding the influence of several atmospheric parameters on the emergent fractional linear polarization profiles. The shapes of these  $Q/I$  profiles are interpreted in terms of the anisotropy of the radiation field, which in turn depends on the source function gradient that sets the angular variation of the specific intensity. We define a suitable frequency integrated anisotropy factor for PRD that can be directly related to the emergent linear polarization. We show that complete frequency redistribution is a good approximation to model weak resonance lines. We also show that the emergent linear polarization profiles can be very sensitive to the thermal structure of the solar atmosphere and, in particular, to spatial variations of the damping parameter.

*Subject headings:* line : profiles – polarization – radiative transfer – scattering – Sun: atmosphere

---

<sup>†</sup>Presently at Indian Institute of Astrophysics, Koramangala, Bangalore, India

## 1. Introduction

The linearly polarized solar limb spectrum produced by scattering processes in quiet regions of the solar atmosphere (Stenflo & Keller 1997), contains a wealth of information on the physics of scattering and on the thermodynamical and magnetic conditions of the solar atmosphere. The rich structuring of this so-called second solar spectrum and its interpretation has opened a new window in solar physics with great diagnostic potential (e.g., Stenflo 2004, 2006; Trujillo Bueno 2001, 2003, 2009). This linearly polarized spectrum has been measured with high spectral resolution from the UV at 3160 Å to the red at 6995 Å (Gandorfer 2000, 2002, 2005). Using this atlas of the second solar spectrum Belluzzi & Landi Degl’Innocenti (2009) have presented a very useful classification and spectroscopic analysis of the most polarizing atomic lines.

The modeling and physical interpretation of the second solar spectrum requires the application of sophisticated theories of line formation capable of accounting for, in a self-consistent way, the physics of scattering polarization in the presence of magnetic fields. Starting from the principles of quantum electrodynamics, a rigorous theory of the polarization in spectral lines was formulated by Bommier & Sahal-Br  chot (1978) for optically thin lines and by Landi Degl’Innocenti (1983, see also the monograph by Landi Degl’Innocenti & Landolfi 2004) for optically thick lines. This latter theory, which can take into account radiative transfer effects in multi-level atomic systems, lower level polarization, hyperfine structure and level crossings interferences, has been successfully applied to interpret several interesting spectropolarimetric observations (see Trujillo Bueno 2009, for a recent review). However, a limitation of this theory is that it is based on the approximation of complete frequency redistribution (CRD) in scattering (namely, no correlation between the frequencies of the incident and scattered photon). Though this is a suitable approximation for several solar spectral lines (e.g., Manso Sainz & Trujillo Bueno 2003; Trujillo Bueno et al. 2004; Št  p  n & Trujillo Bueno 2010), it is not suitable to model the observed linear polarization patterns in some of the strongest and most prominent lines of the second solar spectrum, like Ca I 4227 Å and Ca II K at 3933 Å. For these and a few other resonance lines one has to take into account the effects of partial frequency redistribution (PRD) in scattering.

An attempt to handle PRD effects within a theoretical framework where the basic results of the CRD density-matrix theory are generalized through the hypothesis of considering the atomic levels as a continuous distribution of infinitely sharp sublevels (the so-called metalevels theory) has been proposed by Landi Degl’Innocenti et al. (1997). Although this theory has proved to be quite successful for some applications (e.g., Landi Degl’Innocenti 1998) the difficulty of coherently incorporating depolarizing collisional effects in such a theo-

retical approach prevents us from employing it in the present investigation. We thus prefer, in this paper, to rely on the better-established theory of resonance scattering (see below) although we have to remind that such a theory suffers from the main limitation of being applicable only for two-level atoms with unpolarized, infinitely sharp lower-levels.

In a scattering event, the direction, frequency, and polarization of the scattered photon are in general different from those of the incident photon. The correlations between angle, frequency and polarization of the incident and scattered photons can be described by a PRD matrix. The effects of PRD are clearly observable in the wings of strong resonance lines and to a lesser extent in the line core (e.g., Frisch 1996). The general problem of redistribution of resonance radiation including the effects of collisions was investigated by Omont et al. (1972). Using a quantum mechanical description of matter and radiation, they derived PRD functions in the rest frame of the atom. A year later, these authors addressed the same problem but for the magnetized case (Omont et al. 1973). Starting from the work of Omont et al. (1972), Domke & Hubeny (1988) derived expressions of the PRD matrices for resonance line polarization in a two-level atom with unpolarized lower-level. By applying a master equation theory, Bommier (1997a) derived a more elegant but equivalent expression for the non-magnetic PRD matrix. Furthermore, she derived the explicit form of the laboratory frame PRD matrix in the presence of an arbitrary magnetic field (see Bommier 1997b), for the case of a two-level model atom without atomic polarization in the lower level. Bommier & Stenflo (1999) developed a classical time-dependent oscillator PRD theory for the particular case of a normal Zeeman triplet in the atomic rest frame. The ensuing laboratory frame PRD matrices for the magnetized case were derived by Sampoorna et al. (2007a,b). In this paper we restrict our attention to the problem of resonance line polarization in situations where the radiation field is axially symmetric (e.g., the case of non-magnetic resonance line polarization in plane-parallel stellar atmospheres). We use the angle-averaged (AA) version of the non-magnetic PRD matrix (see Domke & Hubeny 1988; Bommier 1997b).

Dumont et al. (1977) carried out model calculations of polarized line transfer with PRD in axi-symmetric plane-parallel atmospheres. They used the angle-dependent type I (pure Doppler) redistribution function of Hummer (1962), which may be used in some circumstances for the Doppler cores of resonance lines. They considered (1) an isothermal model atmosphere and (2) a chromospheric-like model atmosphere described by an analytic form for the Planck function. For the case of isothermal model atmospheres they studied the influence of  $\epsilon$  (the photon destruction probability per scattering event) and the error introduced by the assumption of CRD on the emergent linear polarization profiles. They showed that CRD is adequate to describe the line core polarization. For the case of schematic chromospheric-like model atmospheres, they considered the influence of the line strength, but under the assumption of CRD. Rees & Saliba (1982, see also Saliba 1985, 1986) consid-

ered the same problem, but using an AA type II redistribution function ( $R_{\text{II,AA}}$ ) of Hummer (1962). However, for  $R_{\text{II,AA}}$  they used an approximate form given by Kneer (1975), which assumes that CRD prevails in the line core and coherent scattering in the wings. They studied the influence of the line strength,  $\epsilon$  and damping parameter  $a$  of the absorption profile on the emergent linear polarization and showed that in the presence of a background continuum, linear polarization profiles with both core and wing maxima are formed in isothermal as well as in chromospheric-like model atmospheres.

Later, Faurobert (1987, 1988) studied the linear polarization of resonance lines formed in isothermal slabs of finite thickness, in semi-infinite isothermal atmospheres and in chromospheric-like model atmosphere. She considered both angle-dependent and AA type II redistribution functions of Hummer (1962). She confirmed the conclusion of Dumont et al. (1977), namely, that the approximation of CRD is adequate to describe the line core polarization even when type II redistribution is used. Using the actual functional form of  $R_{\text{II,AA}}$ , Faurobert (1987, 1988) demonstrated that Kneer’s approximation used by Rees & Saliba (1982) and Saliba (1985, 1986) cannot account for the phenomenon of diffusion in frequency which takes place in the line wings. She showed that Kneer’s approximation leads to non-negligible errors in the wing polarization obtained from slabs of finite thickness. In the case of a semi-infinite atmosphere this approximation affects both the line core and line wing polarization, as well as the intensity itself. Furthermore, she showed that in the presence of a background continuum, Kneer’s approximation predicts incorrect values for both the position and the magnitude of the polarization maximum in the wings. Faurobert (1988) considered also the influence of  $\epsilon$  and of the line strength on the linear polarization profiles and gave a qualitative interpretation of the behavior of the emergent polarization profiles in terms of an Eddington-Barbier expression.

The collisional redistribution matrix given by Domke & Hubeny (1988) was used in polarized line transfer computations by Faurobert-Scholl (1992, in plane-parallel atmospheres) and by Nagendra (1994, 1995, in spherically-symmetric atmospheres). Faurobert-Scholl (1992) showed that the line-wing polarization is sensitive to the elastic collisional rate  $\Gamma_{\text{E}}$  while Nagendra (1994) emphasized that the line core polarization is sensitive to the depolarizing collisions parameter  $D^{(2)}$ . Nagendra (1994, 1995) presented a detailed study about the influence of  $\epsilon$ , the damping parameter  $a$ , the elastic collisional rate  $\Gamma_{\text{E}}$  and  $D^{(2)}$  on the linear polarization profiles, interpreting them using simple asymptotic expression (see e.g., Hubeny 1985a; Frisch 1980).

In all the above-mentioned references, Feautrier’s method was used to solve the PRD polarized line transfer equation, except in Nagendra (1994, 1995) who used a discrete space method. As is well-known, these type of numerical methods are computationally expen-

sive. Over the last two decades fast iterative methods based on operator-perturbation have been developed to solve the PRD radiative transfer problem of resonance line polarization assuming a two-level model atom without lower-level atomic polarization (see the review by Nagendra & Sampoorna 2009). More recently, Sampoorna & Trujillo Bueno (2010) have developed very efficient and accurate symmetric Gauss-Seidel and Successive-Overrelaxation iterative methods to solve the above-mentioned PRD problem. Applying this fast radiative transfer method, in this paper we study in detail the effects of various atmospheric parameters on the linear polarization profiles formed under PRD conditions, but using semi-empirical models of the solar atmosphere and paying particular attention to understanding the shape of the emergent fractional linear polarization profiles in terms of the radiation field anisotropy within the medium. In particular, we consider two one-dimensional (1D) models of the quiet solar atmosphere: one based on the VALC model of Vernazza et al. (1981, which has a relatively hot lower chromosphere) and the second based on the MCO model of Avrett (1995, which has a relatively cool lower chromosphere). Although the solar atmosphere is highly inhomogeneous and dynamic and such 1D models can only be considered as illustrative of the complex atmospheric conditions, they are suitable for achieving the main aim of this paper, namely a basic investigation on the impact of PRD effects on the shape of the emergent  $Q/I$  profiles and their sensitivity to various atmospheric parameters. In particular, we study the sensitivity of the linear polarization profiles to the following relevant quantities: (a) the photon destruction probability per scattering event  $\epsilon$ , (b) the strength of the spectral line, parameterized as  $r$  (see the discussion below Equation (8) for the definition of  $r$ ), (c) the damping parameter  $a$  of the line absorption profile, and (d) the elastic collisional rate  $\Gamma_E$ .

The paper is organized in the following manner: in Section 2 we present a historical background on the PRD matrix for non-magnetic resonance scattering in a two-level atom. The formulation of the problem is presented in Section 3. A detailed study of the sensitivity of the linear polarization profiles to various atmospheric parameters and to the thermal structure of the solar atmosphere is presented in Section 4. Concluding remarks are given in Section 5.

## 2. Redistribution Matrix for the Non-magnetic Resonance Scattering Problem

In this section we present a brief background on the PRD matrix for resonance line polarization. We follow the same notation as in Sampoorna & Trujillo Bueno (2010).

The two-level atom PRD problem without polarization was formulated by Hummer (1962). Later, starting from the work of Omont et al. (1972), more general PRD functions

including a better treatment of collisions, for both resonance and subordinate lines, were derived by Heinzl (1981), Hubeny (1982), Hubeny et al. (1983a,b), Hubeny & Cooper (1986) and Hubeny & Lites (1995). Reviews on the unpolarized PRD problem and its application to astrophysics were presented by Hubeny (1985b) and Frisch (1988). For a more recent review on the same topic, but with emphasis on numerical methods and radiative transfer modeling, see Uitenbroek (2003).

When the polarization state of the spectral line radiation is taken into account the unpolarized PRD functions become  $4 \times 4$  redistribution matrices that describe how the Stokes vector is redistributed in both frequency and angle. In the non-magnetic case the redistribution matrix, once averaged over the Maxwellian distribution of the scattering atoms, can be expressed as a product of the angle and frequency dependent PRD function of Hummer (1962) times a frequency-independent  $4 \times 4$  phase matrix. Clearly, there is an intricate coupling between the frequency, angle and polarization state of the radiation field.

A  $4 \times 4$  phase matrix for the  $J_l = 0 \rightarrow J_u = 1 \rightarrow J_l = 0$  scattering transition was derived by Chandrasekhar (1950) using classical electrodynamics, which is referred to as the Rayleigh phase matrix. Using quantum mechanics Hamilton (1947) derived a more general Rayleigh phase matrix for a  $J_l \rightarrow J_u \rightarrow J_l$  transition with arbitrary values for the lower and upper level angular momentum quantum numbers. For the particular case of a 1D atmosphere, the  $4 \times 4$  phase matrix reduces to a  $2 \times 2$  phase matrix, due to the azimuthal symmetry of the problem.

In polarized radiative transfer, using redistribution matrices that have intricate couplings between frequency and angles is numerically expensive. Hence, to reduce the numerical work, Rees & Saliba (1982) introduced the so-called hybrid approximation, in which it is assumed that the  $4 \times 4$  redistribution matrix, depending on directions and frequencies, can be factorized into a  $4 \times 4$  matrix, depending only on directions, times a scalar function depending only on frequencies (the so-called AA redistribution function). Indeed such a factorization is valid only in the atomic frame. In the laboratory frame it is mainly used as a practical “ansatz” for avoiding extremely time-consuming calculations and is justified only by means of heuristic arguments. Under the hybrid approximation, in a plane parallel atmosphere, the redistribution matrix can be written, in general, as a linear combination of terms of the form<sup>1</sup>

---

<sup>1</sup>Note that the only difference with Equations (33) and (37) of Sampoorna & Trujillo Bueno (2010) is that in Equations (1) and (3) of the present paper we have written  $\phi_x g_{xx'}^k$  instead of  $g_{xx'}^k$ , in order to be consistent with the definition of  $\mathbf{R}$  given below.

$$\mathbf{R}(x, x'; \mu, \mu') = (1 - \epsilon) \phi_x g_{xx'}^k \mathbf{P}(\mu, \mu'). \quad (1)$$

Here  $x, x'$  are the non-dimensional frequencies of outgoing and incoming photons, and  $\mu, \mu'$  are the cosine of the polar angles  $\theta, \theta'$  with respect to the vertical direction in the atmosphere.  $\mathbf{R}(x, x'; \mu, \mu')$  gives the joint probability of absorbing a photon with frequency  $x'$  and direction  $\mu'$  and re-emitting by spontaneous de-excitation a photon with frequency  $x$  and direction  $\mu$ . The photon destruction probability is given by  $\epsilon = \Gamma_I / (\Gamma_I + \Gamma_R)$  with  $\Gamma_I$  being the inelastic de-excitation collision rate and  $\Gamma_R$  the radiative de-excitation rate. In Equation (1),  $g_{xx'}^k = R_{k,AA}(x, x') / \phi_x$ , where  $R_{k,AA}$  (with  $k = \text{I, II, and III}$ ) are the AA redistribution functions of Hummer (1962) and  $\phi_x$  is the normalized Voigt profile function. The function  $R_{k,AA} / \phi_x$  gives the probability of absorption at frequency  $x'$ , per emission at frequency  $x$ . Note that in Equation (1) we introduce for convenience the quantity  $g_{xx'}^k$  which has the advantage of formally simplifying the expression for the line source vector (see Equations (9) and (10) below). Finally, for the case of a 1D atmosphere,  $\mathbf{P}(\mu, \mu')$  denotes the  $2 \times 2$  phase matrix.

The redistribution matrix given in Equation (1) does not take into account the elastic collisions, quantified by the parameters  $\Gamma_E$  and  $D^{(2)}$ . However, the elastic collisional rate  $\Gamma_E$  can be included into the hybrid approximation by replacing  $g_{xx'}^k$  by a linear combination of type II and type III PRD functions, weighted by the factor  $\gamma = (\Gamma_R + \Gamma_I) / (\Gamma_R + \Gamma_I + \Gamma_E)$ , namely

$$\mathbf{R}(x, x'; \mu, \mu') = (1 - \epsilon) \phi_x [\gamma g_{xx'}^{\text{II}} + (1 - \gamma) g_{xx'}^{\text{III}}] \mathbf{P}(\mu, \mu'). \quad (2)$$

We remark that the (1,1) element of  $\mathbf{R}$  given in Equations (1) and (2) is normalized to  $(1 - \epsilon)$ , because it does not take into account the depolarizing collisional rate  $D^{(2)}$ . We refer the reader to Omont et al. (1972) for a detailed discussion on the normalization of the redistribution matrix. To qualitatively model the solar Ca II K line Saliba (1985) used the redistribution matrix given by Equation (2), but with a further simplification which consisted in replacing  $R_{\text{II},AA}$  by Kneer's (1975) approximation and  $R_{\text{III},AA}$  by the CRD expression. Also, he neglected  $\Gamma_I$  in the expression for  $\gamma$  (see above), and assumed that the matrix  $\mathbf{P}(\mu, \mu')$  which multiplies  $R_{\text{III},AA}$  (see Equation (2)) is the isotropic scattering phase matrix. Moreover, Saliba (1985) did not take into account the depolarizing collisional rate  $D^{(2)}$  in his modeling.

The redistribution matrix given by Domke & Hubeny (1988) for the unmagnetized case (see also Bommier 1997b) takes into account the effect of depolarizing collisions through the  $D^{(2)}$  parameter. It is worth noting that this collisional redistribution matrix is very general, namely, it depends on the angle-dependent redistribution functions of Hummer (1962). However, for computational simplicity, following Rees & Saliba (1982), some authors have used

the AA version of this general collisional redistribution matrix (e.g., Faurobert-Scholl 1992; Nagendra 1994). Following Bommier (1997b) the AA version of the collisional redistribution matrix can be written as (see also Equation (37) of Sampoorna & Trujillo Bueno 2010)

$$\begin{aligned} \mathbf{R}(x, x'; \mu, \mu') &= \sum_{K=0,2} W_K(J_l, J_u) \\ &\times \phi_x \{ \alpha g_{xx'}^{\text{II}} + [\beta^{(K)} - \alpha] g_{xx'}^{\text{III}} \} \mathbf{P}_{\text{R}}^K(\mu, \mu'), \end{aligned} \quad (3)$$

where the branching ratios  $\alpha$  and  $\beta^{(K)}$  are given by

$$\alpha = \frac{\Gamma_{\text{R}}}{\Gamma_{\text{R}} + \Gamma_{\text{I}} + \Gamma_{\text{E}}}, \quad (4)$$

$$\beta^{(K)} = \frac{\Gamma_{\text{R}}}{\Gamma_{\text{R}} + \Gamma_{\text{I}} + D^{(K)}}. \quad (5)$$

Note that  $D^{(0)} = 0$ , and also that the factor  $(1 - \epsilon)$  is contained in the branching ratios. The coefficient  $W_0(J_l, J_u) = 1$ , and  $W_2(J_l, J_u)$  characterizes the maximum linear polarization that can be produced in the line. In the case of a normal Zeeman triplet ( $J_l = 0, J_u = 1$ ),  $W_2(J_l, J_u) = 1$ . Furthermore,  $\mathbf{P}_{\text{R}}^K(\mu, \mu')$  are the Rayleigh phase matrix multipolar components (Landi Degl’Innocenti 1984, see also Equation (35) of Sampoorna & Trujillo Bueno 2010).

The CRD limit is obtained from Equation (3) by taking  $\Gamma_{\text{E}} \gg \Gamma_{\text{R}}$  (in other words  $\alpha \ll 1$ ) and  $g_{xx'}^{\text{III}} = \phi_{x'}$  (compare the resulting expression with Equation (10.54) of Landi Degl’Innocenti & Landolfi 2004, with the magnetic field strength set to zero). Notice that CRD means that there is no frequency correlation between the incoming and outgoing photons. In other words, the incident radiation is completely redistributed in frequency, so that there is complete non-coherence between the incident and scattered photon frequencies. This CRD limit is reached when the atomic system is illuminated by a spectrally flat radiation field (e.g., Landi Degl’Innocenti & Landolfi 2004). Another good approximation to this CRD limit occurs when the atoms are so strongly perturbed by elastic collisions during the scattering process that the excited electrons are randomly redistributed over the substates of the upper level (see Mihalas 1978). However, in the context of polarization, adopting the CRD approximation appears to lead to the following contradiction: CRD is obtained in the limit of very high collisional rates with respect to the radiative rate, but then the spectral line would be completely depolarized by depolarizing collisions. This apparent contradiction can be clarified by recalling the explicit physical meaning of the branching ratios appearing in Equation (3). First of all, for the problem at hand, elastic collisions produce two different effects represented by the collisional rates  $\Gamma_{\text{E}}$  and  $D^{(2)}$ . The collisional rate  $\Gamma_{\text{E}}$  is responsible for line broadening and for destruction of correlations between incoming and outgoing photon frequencies. The rate  $D^{(2)}$  is responsible for the destruction of the upper-level atomic



alignment and, thereby, causes depolarization. The branching ratio  $\alpha$  gives the probability that a radiative decay from the excited state occurs before any type of collision (elastic or inelastic). Therefore,  $\alpha$  gives the fraction of the scattering processes that are coherent in the atomic rest frame ( $R_{\text{II}}$ ). The branching ratio  $\beta^{(K)}$  gives the probability that radiative decay of the excited state occurs without destruction of the  $2K$ -multipole moment. Therefore, the total branching ratio  $[\beta^{(K)} - \alpha]$  gives the probability that radiative de-excitation occurs after a elastic collision ( $\Gamma_{\text{E}}$ ) which redistributes the radiation in frequency without destroying the  $2K$ -multipole moment. Clearly  $[\beta^{(K)} - \alpha]$  gives the fraction of the scattering processes that are completely non-coherent in the atomic rest frame ( $R_{\text{III}}$ ). Therefore, to get the CRD limit we only assume that elastic collisions that completely redistribute the radiation in frequency are sufficiently strong ( $\Gamma_{\text{E}} \gg \Gamma_{\text{R}}$ ), so that the branching ratio  $\alpha \rightarrow 0$ . In other words,  $D^{(2)}$  and  $\Gamma_{\text{E}}$  are assumed to be independent, even though their physical origin are the elastic collisions. In this case Equation (3) reduces to

$$\begin{aligned} \mathbf{R}_{\text{CRD}}(x, x'; \mu, \mu') &= \sum_{K=0,2} W_K(J_l, J_u) \\ &\times \beta^{(K)} \phi_x \phi_{x'} \mathbf{P}_{\text{R}}^K(\mu, \mu'), \end{aligned} \quad (6)$$

where we have further replaced  $g_{xx'}^{\text{III}}$  by  $\phi_{x'}$ . Clearly the branching ratio  $\beta^{(K)}$  allows only that fraction of the scattering processes which do not lead to destruction of the  $2K$ -multipole moment.

We compute the  $R_{\text{II,AA}}$  and  $R_{\text{III,AA}}$  functions by numerically integrating the corresponding angle-dependent redistribution functions (see Equations (59) and (61) of Bommier 1997b) over all the scattering angles (see Equations (103) and (104) of Bommier 1997b). For the numerical integration over all the scattering angles we have used a 15 point Gauss-Legendre quadrature. In this paper we assume that the redistribution functions  $R_{\text{II,AA}}$  and  $R_{\text{III,AA}}$  and the Voigt profile function  $\phi_x$  are constant throughout the atmosphere. Since these functions depend on the damping parameter  $a$  and on the reduced frequency  $x$ , which is defined as  $x = (\nu_0 - \nu)/\Delta\nu_{\text{D}}$ , with  $\nu_0$  the line center frequency and  $\Delta\nu_{\text{D}}$  the Doppler width, the above assumption implies that  $a$  and  $\Delta\nu_{\text{D}}$  are also constant within the entire atmosphere.

### 3. Formulation of the Problem

In this section we discuss all the physical ingredients required for our investigation (presented in Section 4) about PRD scattering polarization profiles. Section 3.1 describes the basic equations of the problem. The model atmospheres used for our study in Section 4 are discussed in Section 3.2. The definition of the anisotropy factor for PRD is considered in Section 3.3, where we also discuss several known facts about the anisotropy and its relation

to the source function gradient. In Section 3.4 we present the Eddington-Barbier relation for PRD problems, and show the direct dependence of the emergent polarization on the anisotropy within the model atmosphere under consideration.

### 3.1. The Basic Equations

We consider the standard two-level atom resonance line polarization problem in a one-dimensional, plane-parallel, static stellar atmosphere. Furthermore, we assume an unpolarized background continuum with no continuum scattering. The basic equations for the above-mentioned problem have been presented in detail in Sampoorna & Trujillo Bueno (2010, see their Section 5). Here we follow the same formulation, but for the sake of clarity we recall a few important basic equations from that paper.

As shown by Chandrasekhar (1950), an azimuthally symmetric polarized radiation field can be described by the two Stokes parameters  $I_{x\mu}$  and  $Q_{x\mu}$ . The Stokes  $I_{x\mu}$  parameter is the specific intensity, while  $Q_{x\mu}$  quantifies the linear polarization (i.e., the difference between the intensity components parallel and perpendicular to a given reference direction in the plane perpendicular to the direction of the ray under consideration). In this paper, the positive  $Q_{x\mu}$  direction is defined in the plane containing the direction of the ray and the vertical Z-axis. When polarization is taken into account, the Stokes source vector depends not only on the frequency  $x$  but also on  $\mu = \cos \theta$ , with  $\theta$  the angle between the ray and the vertical Z-axis. It is possible to transform from the Stokes basis to an irreducible basis where the source vector components depend only on the frequency  $x$ . Such a transformation is referred to as the “decomposition” of the Stokes vector. Frisch (2007) has given a simple way of achieving this goal using the irreducible tensors for polarimetry introduced by Landi Degl’Innocenti (1984). This decomposition technique was used in Sampoorna & Trujillo Bueno (2010), and we adopt it here also.

In the reduced basis the irreducible intensity  $(I_{x\mu})_0^K$  with  $K = 0$  and 2 satisfies the following transfer equation

$$\frac{d}{d\tau_{x\mu}}(I_{x\mu})_0^K(\tau_{x\mu}) = (I_{x\mu})_0^K(\tau_{x\mu}) - (S_x)_0^K(\tau_{x\mu}), \quad (7)$$

where the irreducible source vector components are given by

$$(S_x)_0^K = \frac{\phi_x(S_{lx})_0^K + rBU_0^K}{\phi_x + r}. \quad (8)$$

Here  $\tau_{x\mu}$  is the total optical depth defined by  $d\tau_{x\mu} = -(\chi_l\phi_x + \chi_c)dz/\mu$ , with  $z$  the distance along the normal to the atmosphere,  $\chi_l$  and  $\chi_c$  are the line and continuum opacities,  $r =$

$\chi_c/\chi_l$ ,  $B$  is the Planck function, and  $U_0^K$  is equal to unity for  $K = 0$  and zero for  $K = 2$ . The irreducible line source vector components are given by

$$(S_{lx})_0^K = \epsilon B U_0^K + W_K(J_l, J_u)(\bar{J}_x)_0^K, \quad (9)$$

where

$$(\bar{J}_x)_0^K = \int_{-\infty}^{+\infty} dx' \{ \alpha g_{xx'}^{\text{II}} + [\beta^{(K)} - \alpha] g_{xx'}^{\text{III}} \} (J_{x'})_0^K. \quad (10)$$

The angle integrated irreducible tensors of the radiation field are respectively given by

$$(J_x)_0^0 = \frac{1}{2} \int_{-1}^{+1} d\mu I_{x\mu}, \quad (11)$$

$$(J_x)_0^2 = \frac{1}{4\sqrt{2}} \int_{-1}^{+1} d\mu [(3\mu^2 - 1)I_{x\mu} + 3(\mu^2 - 1)Q_{x\mu}]. \quad (12)$$

The irreducible components of the radiation field and of the source function are connected to the Stokes parameters and to the source vector through a simple formula (see Appendix B of Frisch 2007). Note that in the solar atmosphere the dominant contribution to  $(J_x)_0^2$  is given by the first term in the square bracket of Equation (12).

### 3.2. The Model Atmospheres

In this section we describe the two solar model atmospheres that we have chosen for our detailed study of the linear polarization profiles presented in Section 4. As already mentioned in Section 1, we consider the VALC and the MCO models for this purpose. Figure 1 shows the variation of the temperature as a function of height for the VALC (dotted line) and MCO (solid line) models. We note that both models include the transition region as well as the corona. Most of the results presented in this paper correspond to spectral lines which become optically thin for heights  $z > 2100$  km. However, we also present some results for a very strong spectral line whose line center originates in the transition region of the VALC model.

For a hypothetical line at  $\lambda = 5000 \text{ \AA}$  we calculate the Planck function  $B$  (in  $\text{erg s}^{-1} \text{ cm}^{-2} \text{ sr}^{-1} \text{ cm}^{-1}$ ) as<sup>2</sup>

$$B = \frac{2hc^2}{\lambda^5} \frac{1}{e^{hc/(\lambda k_B T)} - 1}, \quad (13)$$

---

<sup>2</sup>Rigorously speaking, the Planck function expression should be that corresponding to the Wien limit because we are neglecting stimulated emission. However, for visible and UV lines both expressions give similar values.

where  $c$  is the speed of light,  $h$  is the Planck constant, and  $k_B$  is the Boltzmann constant. As the tabulated height grid of the VALC and MCO models is crude, we actually first interpolate the tabulated temperatures on a much finer height grid. We use cubic spline interpolation for this purpose. Our height grid has a spacing of  $\Delta z = 5$  km. Note that achieving the accuracy corresponding to such a fine spatial grid requires finding the self-consistent solution via the application of a highly-convergent iterative scheme, such as that on which the PRD computer program used here is based on (see Sampoorna & Trujillo Bueno 2010).

We assume that both solar model atmospheres are exponentially stratified, so that the continuum optical depth is described by the law  $\tau_c = 2.2 \exp(-z/H)$  with  $z$  (in km) the vertical height in the atmosphere, and  $H$  the scale height (which we have chosen equal to 120 km). Moreover, we assume that the line strength parameter  $r$ , the photon destruction probability per scattering  $\epsilon$ , and the damping parameter  $a$  of the line absorption profile are constant with height. Figure 2 shows a plot of  $\tau_c$  versus height for the VALC model. For  $\tau_c$  we use the tabulated value at  $\lambda = 5000 \text{ \AA}$  from Vernazza et al. (1981). Overplotted is our continuum optical depth versus height. Clearly, the  $\tau_c$  of the VALC model does not show a single scale height. In fact, our attempts to fit the  $\tau_c$  of VALC required the use of a weighted combination of two exponentials with two different scale heights. We find that for heights lower than 600 km one has to use a scale height of 60 km, while for larger heights one needs a scale height of 250 km, in order to reasonably fit the  $\tau_c$  of VALC. However, to keep the problem as simple as possible, we choose a single scale height of 120 km for the entire atmosphere and  $\tau_0^c = 2.2$  that nearly coincides with the  $\tau_c$  value of the VALC model at the lower boundary of the atmosphere (see dotted line in Figure 2). The same choice applies to the MCO model. This strategy appears to be reasonable for facilitating a systematic investigation on the impact of PRD effects on the shape of the emergent  $Q/I$  profiles.

### 3.3. The Anisotropy

The  $(J_x)_0^2$  tensor, which is dominated by the contribution from the Stokes  $I_{x\mu}$  parameter, characterizes the ‘degree of anisotropy’ of the radiation field (Landi Degl’Innocenti & Landolfi 2004, see also Trujillo Bueno 2001). We define a ‘monochromatic anisotropy factor’ as

$$A = (J_x)_0^2 / (J_x)_0^0. \quad (14)$$

For clarity of notation, we denote the monochromatic anisotropy  $A$  for CRD and PRD by  $A_{\text{CRD}}$  and  $A_{\text{PRD}}$ , respectively. We also define a ‘frequency integrated or mean anisotropy factor’ for PRD as

$$\bar{A}_{\text{PRD}} = (\bar{J}_x)_0^2 / (\bar{J}_x)_0^0, \quad (15)$$

where  $(\bar{J}_x)_0^0$  and  $(\bar{J}_x)_0^2$  are defined as in Equation (10). In the case of CRD the frequency integrated anisotropy factor is defined by

$$\bar{A}_{\text{CRD}} = (\bar{J}_0^2)_{\text{CRD}} / (\bar{J}_0^0)_{\text{CRD}}, \quad (16)$$

where

$$(\bar{J}_0^K)_{\text{CRD}} = \int_{-\infty}^{+\infty} \beta^{(K)} \phi_x (J_x)_0^K dx. \quad (17)$$

Clearly, the mean anisotropy  $\bar{A}_{\text{CRD}}$  does not depend explicitly on frequency. However, in the solar atmosphere  $\bar{A}_{\text{CRD}}$  changes with height. It then results that, even in CRD, since different points of the profile form at different heights, we have an “apparent” frequency dependence of  $\bar{A}_{\text{CRD}}$  across the profile. On the contrary,  $\bar{A}_{\text{PRD}}$  depends explicitly on frequency and this effect adds to the previous one.

In Figure 3 we illustrate the important difference between the monochromatic and mean anisotropy factors for both, the PRD and CRD cases. To compute these anisotropy factors we have used the VALC model atmosphere (see Section 3.2) and  $\epsilon = 10^{-4}$ ,  $r = 10^{-5}$ ,  $a = 10^{-3}$  and  $\Gamma_{\text{E}}/\Gamma_{\text{R}} = D^{(2)}/\Gamma_{\text{R}} = 0$ . In Figure 3 we plot  $A$  and  $\bar{A}$  versus the reduced frequency at the height where for a line-of-sight (LOS) with  $\mu = 0.11$  the condition  $\tau_{x\mu} = 1$  is satisfied. Clearly, the monochromatic anisotropy factors  $A_{\text{CRD}}$  and  $A_{\text{PRD}}$  are similar. The differences are basically due to the slight differences that are found in Stokes  $I_{x\mu}$  for CRD and PRD (compare the dotted lines in the intensity panels of Figures 4 and 5). It is interesting to note that  $A_{\text{CRD}}(\tau_{x\mu} = 1)$  does not tend to zero in the wings. This is because the condition  $\tau_{x\mu} = 1$  for a LOS with  $\mu = 0.11$  is satisfied at the height of 360 km for all frequencies  $x \geq 20$ . At this height the anisotropy  $A_{\text{CRD}}$  for  $x \geq 20$  is determined by the Planck function gradient at that height. The mean anisotropy factors  $\bar{A}_{\text{PRD}}$  and  $\bar{A}_{\text{CRD}}$  differ greatly, particularly in the wings. This can be understood as follows. In the case of CRD we integrate  $(J_x)_0^2$  and  $(J_x)_0^0$  over all  $x$  after multiplying them by the absorption profile function  $\phi_x$  (see Equation (17)), which goes to zero in the wings. Thus, at any depth  $\tau_{x\mu}$  the dominant contribution to  $(\bar{J}_0^K)_{\text{CRD}}$  and, thereby to  $\bar{A}_{\text{CRD}}$  comes from the line core region. Furthermore, the monochromatic anisotropy  $A_{\text{CRD}}$  decreases with depth, particularly in the line core. As already noted above, the frequency dependence of  $\bar{A}_{\text{CRD}}$  is due to the fact that different parts of the line profile are formed at different heights. Combining these facts, it is easy to see that  $\bar{A}_{\text{CRD}}$  at  $\tau_{x\mu} = 1$ , decreases as the frequency increases. In particular, far in the wings of strong lines like the one we are considering in Figure 3 (i.e., with  $r = 10^{-5}$ )  $\bar{A}_{\text{CRD}}$  is zero (even if  $A_{\text{CRD}}$  is substantial), because we are looking deep in the atmosphere where  $A_{\text{CRD}}$  in the line core is zero (which dominantly contributes to  $\bar{A}_{\text{CRD}}$ ). In the case of PRD, we integrate  $(J_x)_0^2$  and  $(J_x)_0^0$  over all  $x$  after multiplying them by the type II redistribution function (see Equation (10)), which behaves like CRD in the core and like coherent scattering in the wings. Thus, unlike CRD,

at any depth  $\tau_{x\mu}$  the mean anisotropy  $\bar{A}_{\text{PRD}}$  depends explicitly on  $x$ . Furthermore, in the line core it looks somewhat similar to  $\bar{A}_{\text{CRD}}$ . But in the wings  $\bar{A}_{\text{PRD}}$  coincides with  $A_{\text{PRD}}$ , due to the coherent behavior of  $g_{xx'}^{\text{II}}$ .

The importance of the anisotropy factor, which is the fundamental quantity that determines the shape of the emergent polarization, was realized by Rees & Saliba (1982) who pointed out that the polarization is a mapping of the depth dependence of the anisotropy of the radiation field within the atmosphere. However, they neither quantified nor presented a detailed study of the anisotropy factor. Some information can be found in the PhD thesis of Saliba (1986), who presented a study of the anisotropy for the CRD case (see his Chapter 4). He also illustrated the relation of the anisotropy factor to the source function gradient by considering, in a finite slab atmosphere, a simple piece-wise linear source function. His quantities  $\alpha$  and  $\bar{\alpha}$  are quite similar to our quantities  $A_{\text{CRD}}$  and  $\bar{A}_{\text{CRD}}$ . However, in the case of PRD, Saliba (1986) did not define a mean anisotropy factor  $\bar{A}_{\text{PRD}}$  similar to that defined in our Equations (15) and (10) as he used Kneer’s approximation for  $R_{\text{II,AA}}$ . Nevertheless, he correctly noted that for line core frequencies the anisotropy of the radiation field is controlled by  $\bar{A}_{\text{CRD}}$  and for the line wings it is controlled by  $A_{\text{PRD}}$ . In this paper we show that a better way of defining the anisotropy for the PRD problem is through Equation (15) along with Equations (10)–(12).

A Milne-Eddington atmosphere is a very suitable model to clearly demonstrate the strong dependence of the anisotropy factor on the gradient of the source function for the Stokes  $I_{x\mu}$  parameter (see Section 3 of Trujillo Bueno 2001). The mean anisotropy  $\bar{A}_{\text{CRD}}$  is bounded by  $-1/2 \leq \sqrt{2}\bar{A}_{\text{CRD}} \leq 1$ , the lower and upper bounds being for a purely horizontal radiation field without azimuthal dependence and for a purely vertical illumination, respectively. We summarize the following facts about the anisotropy in a stellar atmosphere:

- (1) The anisotropy is essentially negative for an atmosphere with no or very small gradient in the source function. The negative values of the anisotropy means that the radiation field is predominantly limb-brightened (i.e., predominantly horizontal).
- (2) The larger the source function gradient the larger the anisotropy. Positive anisotropy values imply that the radiation field at the spatial point under consideration is predominantly limb-darkened (i.e., predominantly vertical).

In summary, in a stellar atmosphere the outgoing radiation is predominantly vertical (which makes a positive contribution to  $(\bar{J}_x)_0^2$ ), while the incoming radiation is predominantly horizontal (which makes a negative contribution to  $(\bar{J}_x)_0^2$ ). More precisely, “vertical” rays (i.e., with  $|\mu| > 1/\sqrt{3}$ ) make positive contributions to  $\bar{A}$ , while “horizontal” rays (i.e., with  $|\mu| < 1/\sqrt{3}$ ) make negative contributions to  $\bar{A}$ . As seen in Figure 4 of Trujillo Bueno (2001), the larger the gradient of the source function the greater the anisotropy factor of

the pumping radiation field, and the larger the amount of atomic level polarization. A more detailed study of the anisotropy factor and its relation to the source function gradient can be found in Landi Degl’Innocenti & Landolfi (2004).

More recently, Holzreuter et al. (2005) have presented a study of the monochromatic anisotropy  $A_{\text{PRD}}$  for the solar Ca I 4227 Å and Na I 5890 Å lines taking into account the AA collisional redistribution matrix (see, e.g., Stenflo 1994). They also illustrate the relation of  $A_{\text{PRD}}$  to the source function gradient. However, as they consider only  $A_{\text{PRD}}$  the interpretation of the emergent linear polarization in terms of  $A_{\text{PRD}}$  is not straightforward. In this paper we show that a better quantity that can be directly related to the emergent linear polarization is  $\bar{A}_{\text{PRD}}$ .

### 3.4. The Eddington-Barbier Relation

In the case of CRD, the emergent polarization directly depends on the anisotropy of the radiation field (see Equation (13) of Trujillo Bueno 1999, see also Section 1 of Trujillo Bueno 2003). Such a relation can be considered as the generalization of the Eddington-Barbier relation for scattering polarization. Thus, the emergent polarization is governed by the anisotropy of the radiation field, which in turn is strongly related to the gradient of the source function for Stokes  $I_{x\mu}$  and, therefore, to the  $\mu$  dependence of  $I_{x\mu}$ . Note that the Eddington-Barbier relation given by Trujillo Bueno (1999, 2003) for the CRD problem is very general, as it takes into account the effects of lower-level polarization.

An Eddington-Barbier relation for the PRD case was given by Faurobert (1987, 1988) who used it for a qualitative analysis of the linear polarization profiles formed in an isothermal model atmosphere. According to the Eddington-Barbier relation the emergent intensity and the emergent polarization from a semi-infinite atmosphere can be written as (see also Equation (41) of Frisch et al. 2009)

$$\begin{aligned} I_{x\mu}(\tau_{x\mu} = 0) &\simeq (S_x)_0^0(\tau_{x\mu} = 1), \\ Q_{x\mu}(\tau_{x\mu} = 0) &\simeq \frac{3}{2\sqrt{2}}(\mu^2 - 1)(S_x)_0^2(\tau_{x\mu} = 1). \end{aligned} \quad (18)$$

Restricting to the pure line case, and neglecting the thermal term  $\epsilon B$ , it is easy to show from Equations (9)–(12) and (15), that

$$\left(\frac{Q_{x\mu}}{I_{x\mu}}\right)(\tau_{x\mu} = 0) \simeq \frac{3}{2\sqrt{2}}(\mu^2 - 1) W_2 \bar{A}_{\text{PRD}}(\tau_{x\mu} = 1). \quad (19)$$

This approximate formula shows clearly that the emergent fractional linear polarization depends on the mean anisotropy  $\bar{A}_{\text{PRD}}$  at  $\tau_{x\mu} = 1$  along the LOS. In this paper, we therefore

show  $\bar{A}_{\text{PRD}}$  versus the reduced frequency at the height in the model atmosphere where  $\tau_{x\mu} = 1$  for a LOS with  $\mu = 0.11$ . Furthermore, as our reference direction for positive Stokes  $Q$  is defined perpendicular to the limb, we plot  $-Q/I$  whose positive values indicate polarization parallel to the limb.

#### 4. The Emergent Linear Polarization Profiles

In this section we present a detailed study of the PRD scattering polarization profiles computed in the VALC and MCO model atmospheres (see Section 3.2 for details on the assumptions made). For these two atmospheric models we present our results by giving, for each choice of atmospheric parameters, a set of figures with four panels showing: (a) the emergent intensity at  $\mu = 0.11$  (normalized to the continuum intensity) as a function of the reduced frequency; (b) the emergent fractional linear polarization at  $\mu = 0.11$  as a function of the reduced frequency; (c) the mean anisotropy factor,  $\bar{A}$ , evaluated at the height where the monochromatic optical depth along a LOS with  $\mu = 0.11$  is equal to unity, as a function of reduced frequency; (d) the line source function at line center ( $x = 0$ ) for the intensity propagating along a LOS with  $\mu = 0.11$  (denoted as  $S_I$ ) as a function of height. For the sake of comparison, the corresponding CRD linear polarization profiles are shown for certain cases.

##### 4.1. Results of calculations in the VALC Model

In this section we study the influence of the line strength parameter  $r$ , the photon destruction probability per scattering  $\epsilon$ , the damping parameter  $a$ , the elastic collisional rate  $\Gamma_E$  and the depolarizing rate  $D^{(2)}$  on the PRD linear polarization profiles. We use  $\lambda = 5000 \text{ \AA}$ ,  $\epsilon = 10^{-4}$ ,  $r = 10^{-5}$ ,  $a = 10^{-3}$ , and  $\Gamma_E/\Gamma_R = D^{(2)}/\Gamma_R = 0$  as the nominal case, around which we vary the various parameters mentioned above. Such a study should help us to understand the results of future, more realistic computations where all the above-mentioned parameters are depth dependent. Unless stated otherwise we set  $W_2 = 1$ , which represents the case of a line transition with  $J_l = 0$  and  $J_u = 1$ . For the sake of clarity we divide this section about the results of our radiative transfer calculations in the VALC model in various subsections dealing with the sensitivity of the solution to  $r$  (Section 4.1.1),  $\epsilon$  (Section 4.1.2),  $a$  (Section 4.1.3),  $\Gamma_E/\Gamma_R$  and  $D^{(2)}/\Gamma_R$  (Section 4.1.4). Some additional studies are presented in Section 4.1.5 concerning lines with wavelengths other than  $\lambda = 5000 \text{ \AA}$ , lines formed in the transition region, and lines with other  $W_2$  values.



#### 4.1.1. Effect of the Line Strength Parameter $r$

Figure 4 shows the response of  $I(\tau_{x\mu} = 0)$ ,  $-(Q/I)(\tau_{x\mu} = 0)$ ,  $\bar{A}_{\text{PRD}}(\tau_{x\mu} = 1)$ , and  $S_{\text{I}}(x = 0)$  for a LOS with  $\mu = 0.11$  to variations in  $r$ . For comparison the corresponding CRD case is shown in Figure 5. For notational simplicity we drop the subscripts  $x\mu$  on  $I$  and  $Q$ . Table 1 gives the height in the VALC model atmosphere at which lines of different strengths have  $\tau_{0\mu} = 1$ , both for  $\mu = 0.11$  and  $\mu = 1$ .

We first discuss the PRD line profiles presented in Figure 4 and then compare them with the CRD profiles of Figure 5. Table 1 indicates that as  $r$  decreases we progressively sample lines that are formed higher in the atmosphere. As  $r$  increases the line becomes weaker and the broad damping wings disappear (see Figure 4). The  $-Q/I$  profile of the line with  $r = 10^{-6}$  shows a maximum in both the line core and in the line wing (i.e., at about  $\approx 15$  Doppler widths) as well as a minimum in the near wing (i.e., at about  $\approx 4$  Doppler widths). As  $r$  increases both the wing maximum and the wing minimum are shifted towards line center and decrease in magnitude, to eventually disappear (see the long-dashed line in Figure 4). The line core polarization, however, initially decreases and becomes negative for  $r = 10^{-2}$  and then becomes positive again for  $r = 0.7$ . This response of  $-Q/I$  to the variations in  $r$  can be understood using the mean anisotropy  $\bar{A}_{\text{PRD}}$  plotted in Figure 4. It is worth to note that the shapes of the  $-Q/I$  profiles that we obtain with PRD for  $r$  values between  $10^{-6}$  and  $10^{-2}$  (see Figure 4) are similar to those classified as M-signals by Belluzzi & Landi Degl’Innocenti (2009), whereas the shape of the  $-Q/I$  profile for  $r = 0.7$  is similar to that classified as S-signal by these authors. We recall from Belluzzi & Landi Degl’Innocenti (2009) that a  $Q/I$  profile with a single peak at line center is classified as S-signal, while  $Q/I$  profiles showing a polarization maximum in the wings, a decrease in amplitude approaching the line core, and eventually a narrow peak at line center are classified as M-signals.

For  $r = 10^{-6}$  and  $10^{-5}$  the  $-Q/I$  profile is nearly proportional to  $\bar{A}_{\text{PRD}}$  in the frequency range  $0 \leq x \leq 5$  Doppler widths, so that Equation (19) is applicable. However for  $x > 5$ , one cannot neglect the contribution of  $r$  in  $(S_x)_0^0$  as was done to deduce Equation (19). In the presence of a background continuum, one can approximately write the emergent  $Q/I$  profile as (still neglecting the thermal term  $\epsilon B$ )

$$\frac{Q}{I}(\tau_{x\mu} = 0) \approx \frac{3}{2\sqrt{2}} (\mu^2 - 1) W_2 \frac{\phi_x \bar{A}_{\text{PRD}}(\tau_{x\mu} = 1)}{\phi_x + r B / (\bar{J}_x)_0^0}. \quad (20)$$

The term with  $r$ , in the denominator of Equation (20), is responsible for the formation of a wing maximum in  $-Q/I$ . The fact that the introduction of  $r$  gives rise to a wing maximum in  $-Q/I$  was already noted for isothermal models by Rees & Saliba (1982). This wing maximum is located at the frequency where the radiation field starts being influenced by

the continuous absorption (see Faurobert 1988). In other words, at that frequency the line source function and the (unpolarized) continuum source function equally contribute to the total source function. For isothermal model atmosphere the position of this wing maximum can be estimated using the thermalization frequency given by Frisch (1980).

The frequency range where Equation (19) can be applied decreases as  $r$  increases and can no longer be applied for  $r > 10^{-2}$ . On the other hand, when  $r$  increases, the term containing  $r$  in Equation (20) starts influencing not only the wings but also the line core region, thereby greatly reducing the polarization in the wings to zero and confining the  $-Q/I$  profile to the line core. It is worth to note that for  $r \leq 10^{-3}$  the mean anisotropy  $\bar{A}_{\text{PRD}}$  is positive in the line core and in the line wings showing that the radiation field is limb-darkened. For those frequencies  $x$  whose  $\tau_{x\mu} = 1$  at the heights where we have the VALC temperature rise ( $\approx 500 - 1000$  km; see Figure 1), the anisotropy is negative, showing that the radiation field is limb-brightened. This fact was already noted for schematic chromospheric-like models by Faurobert (1988).

As  $r$  increases, the anisotropy  $\bar{A}_{\text{PRD}}$  in the line core decreases and even becomes negative for  $r = 10^{-2}$ . This is because the line core photons now start to originate in deeper layers of the atmosphere, where the radiation field for the line core photons tends to become more and more isotropic. For  $r = 10^{-2}$  a limb-brightened radiation field dominates to give a negative  $\bar{A}_{\text{PRD}}$  in the line core. However, for  $r = 0.7$ , the anisotropy  $\bar{A}_{\text{PRD}}$  reaches a large positive value. Note that the corresponding line source function  $S_I$  shows a larger departure from the Planck function, not only above the temperature minimum, but also in the photospheric range of heights 300 – 500 km (where actually the line core is formed; see Table 1), differently from what happens with other values of  $r$  (see the  $S_I$  panel of Figure 4). In fact, by taking values of  $r$  between  $10^{-2}$  and 0.7, it can be shown that there is a gradual transition in the line-center anisotropy  $\bar{A}_{\text{PRD}}$  from negative values to a large positive value.

It is worth to note that  $\bar{A}_{\text{PRD}}$  in the wings attains a constant value, which is the same for all the values of  $r$ . However, the frequency distance from line center at which this constant value is reached decreases as  $r$  increases. This can be understood by taking the example of  $r = 10^{-5}$ . In this case we find that the Stokes parameters at all frequencies  $x \geq 20$  are “formed” at a height of 360 km (in the sense that this is the height at which the monochromatic optical depth is unity). When we plot the total source function for all these frequencies we find that they nearly coincide with the Planck function and, moreover, that they are dominated by the continuum source function. Thus, the anisotropy at those frequencies is determined by the Planck function gradient at a height of 360 km. As  $r$  increases the frequency value above which all the photons form at 360 km progressively moves towards line center.

A comparison of Figures 4 and 5, shows that CRD is a good approximation in the line core and particularly at line center. This is a well known result since the detailed work by Dumont et al. (1977, using the type I redistribution function) and Faurobert (1987, 1988, using the type II redistribution function). Furthermore, for sufficiently large values of  $r$  (weak resonance lines) the CRD approximation can be safely used to model line profiles (Frisch 1996), like for instance the  $Q/I$  profiles of the photospheric line of Sr I at 4607 Å (see Faurobert-Scholl 1993). This is because these lines do not have well-developed broad wings (unlike the strong resonance lines). Therefore transfer of photons in the line wings, where frequency coherent scattering can play a crucial role, is negligible (see Faurobert-Scholl 1993). As a result, even in the PRD case, the polarization gets confined to the line core as in the CRD case.

#### 4.1.2. Effect of Photon Destruction Probability Per Scattering $\epsilon$

Figure 6 shows the sensitivity of  $I$ ,  $-Q/I$ ,  $\bar{A}_{\text{PRD}}(\tau_{x\mu} = 1)$  and  $S_{\text{I}}(x = 0)$  at  $\mu = 0.11$  to changes in the  $\epsilon$  value. The corresponding CRD case is shown in Figure 7.

When  $\epsilon$  increases the coupling between the radiation field and the Planck function becomes stronger. From Figure 6 we clearly see that  $S_{\text{I}} \simeq B$  in a greater region of the atmosphere for larger values of  $\epsilon$ . As a result, the intensity increases. However, the anisotropy decreases in the line core. Moreover, for frequencies  $x \simeq 2.5$  the absolute value of the anisotropy (which is here negative) increases, while for  $x > 7$  the anisotropy is independent of  $\epsilon$ . Note that  $x \approx 7$  corresponds to the wing maximum in the  $-Q/I$  profile. As already noted in Section 4.1.1, at this frequency the total source function starts being dominated by the unpolarized continuum, so that the anisotropy as well as  $-Q/I$  are independent of  $\epsilon$ . A comparison with the corresponding CRD case in Figure 7, shows that the above discussion for the line core region can be used to understand the CRD profiles also.

#### 4.1.3. Effect of the Damping Parameter $a$

Figure 8 shows the response of  $I$ ,  $-Q/I$ ,  $\bar{A}_{\text{PRD}}(\tau_{x\mu} = 1)$  and  $S_{\text{I}}(x = 0)$  at  $\mu = 0.11$  to variations of  $a$ . The corresponding CRD case is shown in Figure 9.

The larger the damping parameter  $a$  the broader the absorption profile. As a result the emergent  $I$  as well as  $-Q/I$  profiles broaden as  $a$  increases. Furthermore, an increase of  $a$  implies that the source function departs from the Planck function to a slightly larger extent (see Figures 8 and 9). In the CRD case the anisotropy decreases with increasing values of  $a$

and the  $-Q/I$  profile does the same. In the PRD case the anisotropy at line center does not show a large sensitivity to  $a$ , and thereby the same happens with  $-Q/I$ . On the contrary, for  $x > 3$ ,  $\bar{A}_{\text{PRD}}$  shows a large sensitivity to variations in  $a$ . In particular, the anisotropy increases in absolute value for frequencies that are formed in the temperature rise region of the VALC atmosphere. Furthermore, as  $a$  increases the frequency at which  $\bar{A}_{\text{PRD}}$  reaches a constant value also increases. Consequently the negative dip (or wing minimum) and the wing maximum in  $-Q/I$  are very sensitive to  $a$ . The position of the negative dip as well as that of the wing maximum shifts away from line center. Since the position of the wing maximum is determined by the frequency at which the total source function starts being dominated by the unpolarized continuum, it is clear that an increase in  $a$  results in a shift towards larger frequencies of the wing maximum of  $-Q/I$ . It is worth to note that Saliba (1985) also shows the influence of  $a$  on  $I$  and  $-Q/I$ , though a detailed analysis is missing. Nevertheless, it is clear from our Figure 8 that a height dependence of  $a$  has important effects on the emergent polarization profiles, a point already stressed by Saliba (1985).

We point out that our assumption of a constant damping parameter  $a$  throughout the atmosphere is actually in contradiction with the hypothesis of an exponentially stratified atmosphere. This is because, as  $a$  is proportional to the density, it should also be exponentially stratified. We also point out that the damping parameter  $a$  is proportional to the elastic collisional rate  $\Gamma_{\text{E}}$ , that has been here assumed to be zero. Notwithstanding these inconsistencies, we considered worthwhile to perform our studies as if the damping parameter were an independent quantity.

#### 4.1.4. *Effect of the Elastic Collisions*

Figure 10 shows the sensitivity of  $I$ ,  $-Q/I$ ,  $\bar{A}_{\text{PRD}}(\tau_{x\mu} = 1)$  and  $S_{\text{I}}(x = 0)$  at  $\mu = 0.11$  to the variations of  $\Gamma_{\text{E}}/\Gamma_{\text{R}}$ . The corresponding CRD case is shown in Figure 11. The depolarizing elastic collision parameter is assumed to be  $D^{(2)} = 0.5 \Gamma_{\text{E}}$  (e.g., Stenflo 1994). We recall that in the CRD case, the redistribution matrix is given by Equation (6). Clearly only  $D^{(2)}$  is the relevant quantity for CRD. Therefore, for CRD varying  $\Gamma_{\text{E}}/\Gamma_{\text{R}}$  is equivalent to varying  $D^{(2)}/\Gamma_{\text{R}}$  since we have assumed  $D^{(2)}/\Gamma_{\text{R}} = 0.5 \Gamma_{\text{E}}/\Gamma_{\text{R}}$ . We note that  $\Gamma_{\text{E}}/\Gamma_{\text{R}}$  mainly operates in the line wing, while  $D^{(2)}/\Gamma_{\text{R}}$  operates in the line core (see also Faurobert-Scholl 1992; Nagendra 1994). In the solar atmosphere the elastic collisions  $\Gamma_{\text{E}}$  and  $D^{(2)}$  increase with depth in the atmosphere, while they are negligible in the upper layers, namely in the upper chromosphere and transition region. Thus, depth dependent elastic collisions affect only the wings through  $\Gamma_{\text{E}}/\Gamma_{\text{R}}$ , while the line core is nearly unaffected as it is formed higher in the atmosphere where  $D^{(2)}$  is negligible (see also Faurobert-Scholl 1992).

As expected, elastic collisions have little effect on the line source function  $S_I$ . In the case of PRD, as  $\Gamma_E/\Gamma_R$  operates in the line wings, there is here some sensitivity to this parameter in the intensity profile. However, for CRD, as  $D^{(2)}/\Gamma_R$  operates mainly in the line core, there is hardly any effect on the intensity. As  $\Gamma_E/\Gamma_R$  or  $D^{(2)}/\Gamma_R$  increases, basically the mean anisotropy factors  $\bar{A}_{\text{CRD}}$  and  $\bar{A}_{\text{PRD}}$  decrease at all frequencies. In the case of PRD, with an increase in elastic collisions, the contribution of  $g_{xx}^{\text{III}}$  increases. Since  $g_{xx}^{\text{III}}$  behaves more like CRD, when its contribution increases  $\bar{A}_{\text{PRD}}$  in the wings decreases and it then gradually tends to zero.

#### 4.1.5. Additional Studies

Here we present some additional studies related to the PRD linear polarization profiles. From now on we do not present the corresponding CRD cases.

In Figure 12 we show  $I$ ,  $-Q/I$ ,  $\bar{A}_{\text{PRD}}(\tau_{x\mu} = 1)$  and  $S_I(x = 0)$  at  $\mu = 0.11$  for two different spectral lines. Clearly, the gradient of the Planck function as well as of  $S_I$  are larger at shorter wavelengths (e.g., for  $\lambda = 3933 \text{ \AA}$  compared to those for  $\lambda = 5000 \text{ \AA}$ ), particularly in the photosphere. Therefore, when we move to the blue part of the spectrum the anisotropy increases particularly in the wings, so that the polarization also increases there.

Figure 13 shows  $I$ ,  $-Q/I$ ,  $\bar{A}_{\text{PRD}}(\tau_{x\mu} = 1)$  and the line source function  $S_I(x = 0)$  at  $\mu = 0.11$  for lines formed in the transition region of the VALC model. As  $r$  decreases, the line is formed higher in the atmosphere (see Table 1) where it encounters a steep temperature rise, so that the radiation field tends towards becoming limb-brightened. As a result, the anisotropy decreases in the line core, while it increases in absolute value at the negative dip ( $3 \leq x \leq 7$ ). Moreover, as  $r$  decreases Equation (19) can now be applied to a larger frequency domain and hence the wing maximum in  $-Q/I$ , where the unpolarized continuum source function starts to dominate, now shifts towards larger frequencies. As the spectral line is formed in the region of the steep temperature rise, the intensity shows a typical emission profile, increasingly self-absorbed.

Figure 14 shows the effect of  $W_2$  on  $-Q/I$  and  $\bar{A}(\tau_{x\mu} = 1)$  at  $\mu = 0.11$ , for the VALC model including its transition region and corona. Since  $W_2$  has only marginal effects on the intensity and the line source function  $S_I$ , we do not show them here. As expected, when  $W_2$  decreases the polarization decreases everywhere. However, it is interesting to note that, in general, we expect a linear dependence on  $W_2$  (since  $(S_{lx})_0^2$  directly depends on  $W_2$ , see Equation (9)). In other words, as  $W_2$  is reduced to half, we expect the polarization to be also reduced to half its value throughout the profile when compared to the corresponding  $W_2 = 1$

case. Instead, we see that for  $x < 3$ ,  $-Q/I(W_2 = 0.5)$  is nearly  $0.5 \times -Q/I(W_2 = 1)$ . But for  $x > 3$  there is no linear dependence on  $W_2$ . This can also be seen in the mean anisotropy  $\bar{A}_{\text{PRD}}$ , which does not contain the  $W_2$  factor in its definition (see Equations (10)–(12) and (15)). If there were a linear dependence on  $W_2$ , the mean anisotropy  $\bar{A}_{\text{PRD}}$  should have been exactly the same for both  $W_2 = 0.5$  and  $W_2 = 1$ . Instead, we see considerable difference for  $x > 3$ . This difference can be attributed to the contribution of  $Q$  to  $(\bar{J}_x)_0^2$ , as  $I$  is only marginally affected by the value of  $W_2$ . Thus, we conclude that the scattering polarization depends non-linearly on  $W_2$ . This is true even for the CRD case. This fact was also noted by Stenflo & Stenholm (1976).

## 4.2. Results of Calculations in the MCO Model

Here we study the effect of a relatively cool lower chromosphere on the emergent  $Q/I$ . As the sensitivity to parameters like  $r$ ,  $\epsilon$  and  $a$  is already quite well understood for the VALC model, here we only present: (1) the comparison between the line profiles of VALC and MCO models, and (2) the influence of the elastic collisional rates  $\Gamma_E/\Gamma_R$  and  $D^{(2)}/\Gamma_R$ . We do not show the corresponding CRD case as the main effects are confined to the line core.

Figure 15 shows the effect of the thermal structure of the atmosphere on the polarized line formation. From Figure 1 we see that the temperature minimum is shifted from the height  $z = 500$  km in the VALC model to 1000 km in the MCO model. Thus, monochromatic radiation formed in the region 500 – 1000 km in the VALC model is limb-brightened, while it is limb-darkened in the MCO model (as there is no temperature rise in that region). As the region of temperature rise for the MCO model is located between 1000 and 2000 km, where the line core is formed, we find that the anisotropy in the line core is smaller for the MCO model than for the VALC model. The temperature rise tends to make the radiation field more limb-brightened. Finally, in the wings the anisotropy is smaller compared to that of the VALC model. This is because frequencies  $x \geq 4$  are formed in the region 360 – 500 km, where the temperature gradient is larger for VALC than for MCO.

Figure 16 shows the effect of varying the elastic collisional rate  $\Gamma_E/\Gamma_R$  for the MCO model. Effects of varying  $\Gamma_E/\Gamma_R$  or  $D^{(2)}/\Gamma_R$  for MCO model is more or less similar to that for the VALC model. We note that when  $\Gamma_E/\Gamma_R$  increases, the differences in the anisotropy as well as in the polarization obtained from the MCO and VALC models decrease (for example compare the long-dashed lines in Figures 10 and 16).

## 5. Conclusions

The interpretation of the second solar spectrum is an exciting and tough challenge in Solar Physics. To achieve this it is essential to solve the polarized radiative transfer equation taking into account various physical phenomena. In the case of strong resonance lines one of the important physical ingredients required for the modeling of the linear polarization profiles is the so-called partial frequency redistribution (PRD). In this paper, therefore, we have studied the scattering polarization profiles formed under PRD. We use the angle-averaged version of the collisional redistribution matrix (see Domke & Hubeny 1988; Bommier 1997b), which is valid for a two-level atom with unpolarized lower level. For the numerical method of solution we have applied the very efficient and accurate symmetric Gauss-Seidel method presented in Sampoorna & Trujillo Bueno (2010).

Our main focus in this paper has been to study the influence of various atmospheric parameters (namely,  $\epsilon$ ,  $r$ ,  $a$ ,  $\Gamma_E/\Gamma_R$ ,  $D^{(2)}/\Gamma_R$  and the temperature structure of the atmosphere) on the linear polarization profiles. Interestingly, for strong lines the  $-Q/I$  profiles that we obtain with PRD, for a wide range of the various parameters, are of the shape that has been classified as M-signals by Belluzzi & Landi Degl’Innocenti (2009). We recall that M-signals represent  $Q/I$  profiles with a three-peak structure. Therefore, we find that for strong resonance lines the three-peak structure for  $Q/I$  is a common feature for various combinations of the other relevant parameters, thereby confirming previous results either obtained using more crude model atmospheres (isothermal atmospheres) or with less sophisticated modeling.

We interpret the linear polarization profiles using the Eddington-Barbier relation and the anisotropy at the atmospheric height where  $\tau_{x\mu} = 1$ . To this end, as in the CRD case, we define a suitably frequency integrated or mean anisotropy factor  $\bar{A}$  for PRD, that can be directly related to the emergent linear polarization. We have shown in great detail that the emergent scattering polarization is a mapping of the anisotropy at  $\tau_{x\mu} = 1$  (cf., Rees & Saliba 1982; Trujillo Bueno 2001; Landi Degl’Innocenti & Landolfi 2004). Our study shows that a height dependent damping parameter  $a$  has significant influence on the emergent linear polarization profiles, particularly in the wings of strong resonance lines. In general, scattering polarization profiles are very sensitive to the thermal structure of the atmosphere (see Figure 15). For the range of parameters considered in this paper, we find also that the dips in  $Q/I$  are located at values of reduced frequency  $x$  ranging from 2 to 5. Furthermore, the values of  $Q/I$  at these dips (including their sign) seem to be very sensitive to the thermal structure and to the various atmospheric parameters.

The results of our investigation emphasize that PRD is required to model the linear polarization of strong resonance lines like Ca II K and Mg II k (compare Figures 4 and 5, see

also Figure 13), while CRD is a good approximation to model weak resonance lines like Sr I 4607 Å (see also Faurobert-Scholl 1993; Frisch 1996, and compare the long-dashed lines of our Figures 4 and 5). A strong resonance line is characterized by broad damping wings, where frequency coherent scattering can play a crucial role (e.g., Frisch 1996). Weak resonance lines lack such damping wings and, therefore, the corresponding linear polarization, even computed in PRD, gets confined to the line core, with a single peak at line center, similarly to what is obtained when assuming CRD. In order to quantify the difference between the linear polarization profiles computed with CRD and PRD for the case of weak resonance lines, we define the following two quantities:

$$\delta \left[ \frac{Q}{I}(x=0) \right] = \frac{|(Q/I)_{\text{PRD}}(x=0) - (Q/I)_{\text{CRD}}(x=0)|}{|(Q/I)_{\text{PRD}}(x=0)|}, \quad (21)$$

which gives the relative difference in amplitude of  $Q/I$  computed using CRD and PRD at line center, and

$$\delta [\text{HWHM}] = \frac{|(\text{HWHM})_{\text{PRD}} - (\text{HWHM})_{\text{CRD}}|}{|(\text{HWHM})_{\text{PRD}}|}, \quad (22)$$

which gives the relative difference in the half width at half maximum (HWHM) of the  $Q/I$  profiles computed using CRD and PRD. Taking the particular case of  $r = 0.7$  (see long-dashed lines in Figures 4 and 5), we varied  $\epsilon$ ,  $a$ , and  $\Gamma_{\text{E}}/\Gamma_{\text{R}}$  as done in Figures 6 – 11 for  $r = 10^{-5}$ . We find that  $\delta [(Q/I)(x=0)]$  is around 5% and  $\delta[\text{HWHM}]$  is about 10% for the above-mentioned parametric study with fixed  $r = 0.7$ . Clearly, the error introduced through the use of CRD for weak resonance lines is quite small. Therefore, we may conclude that CRD is a good approximation for weak resonance lines.

Future investigations should extend the present work by considering angle-dependent redistribution functions and the Hanle effect of deterministic magnetic fields. On the one hand, radiative transfer calculations with angle-dependent redistribution functions are numerically very expensive (e.g., Faurobert 1988; Nagendra et al. 2002). To assume the angle-averaged PRD function used here instead of the general angle-dependent function is justified only when polarization is neglected (e.g., Frisch 1996). Since resonance polarization is largely controlled by the anisotropy of the radiation field, the use of angle-averaged functions may not be as suitable for polarized transfer as for non-polarized transfer. Tests of this approximation performed by Faurobert (1988) for purely coherent scattering in semi-infinite isothermal atmospheres show that the errors in the linear polarization are very small in the wings, while in the line core the polarization peak obtained with the angle-dependent type II redistribution function is slightly sharper than with  $R_{\text{II,AA}}$ . However, such tests need to be revised considering more realistic solar model atmospheres. On the other hand, polarized radiative transfer computations of the Hanle effect with angle-averaged PRD have been performed for isothermal model atmospheres by several researchers (e.g., Faurobert-Scholl 1991;



Nagendra et al. 1999; Fluri et al. 2003; Sampoorna et al. 2008b). Even though the Hanle effect is confined to the line core, there are considerable differences in the linear polarization profiles computed using CRD and angle-averaged PRD functions (e.g., Faurobert-Scholl 1991; Nagendra et al. 1999). Furthermore, Nagendra et al. (2002, see also Sampoorna et al. 2008a) have investigated the reliability of angle-averaged functions for the case of Hanle effect in isothermal atmospheres, showing that the Stokes  $U$  parameter is relatively more sensitive than Stokes  $Q$  regarding the use of angle-averaged versus angle-dependent functions. Therefore, to further assess the relative importance of PRD effects, we need to carry out detailed investigations similar to the one reported in this paper but including the Hanle effect of weak magnetic fields. Obviously, such radiative transfer problems are significantly more complicated than the one considered here, but we think that the same numerical method presented in Sampoorna & Trujillo Bueno (2010) can be suitably generalized to solve efficiently such more general PRD problems, both in 1D and 3D geometries.

We are grateful to Luca Belluzzi and to the referee for carefully reviewing our paper. Thanks are also due to Dr. V. Bommier for providing a FORTRAN routine to compute the type III redistribution function and to Dr. K. N. Nagendra for valuable scientific discussions. Financial support by the Spanish Ministry of Science and Innovation through projects AYA2007-63881 (Solar Magnetism and High-Precision Spectropolarimetry) and CONSOLIDER INGENIO CSD2009-00038 (Molecular Astrophysics: The Herschel and Alma Era) is gratefully acknowledged.

## REFERENCES

- Avrett, E. H. 1995, in *Infrared Tools for Solar Astrophysics: What's Next?*, ed. J. R. Kuhn, & M. J. Penn (Singapore: World Scientific), 303
- Belluzzi, L., & Landi Degl'Innocenti, E. 2009, *A&A*, 495, 577
- Bommier, V. 1997a, *A&A*, 328, 706
- Bommier, V. 1997b, *A&A*, 328, 726
- Bommier, V., & Sahal-Br  chot, S. 1978, *A&A*, 69, 57
- Bommier, V., & Stenflo, J. O. 1999, *A&A*, 305, 327
- Chandrasekhar, S. 1950, *Radiative Transfer* (Oxford: Clarendon Press)
- Domke, H., & Hubeny, I. 1988, *ApJ*, 334, 527

- Dumont, S., Omont, A., Pecker, J. C., & Rees, D. E. 1977, *A&A*, 54, 675
- Faurobert, M. 1987, *A&A*, 178, 269
- Faurobert, M. 1988, *A&A*, 194, 268
- Faurobert-Scholl, M., 1991, *A&A*, 246, 469
- Faurobert-Scholl, M., 1992, *A&A*, 258, 521
- Faurobert-Scholl, M., 1993, *A&A*, 268, 765
- Fluri, D. M., Nagendra, K. N., & Frisch, H. 2003, *A&A*, 400, 303
- Frisch, H. 1980, *A&A*, 87, 357
- Frisch, H. 1988, in *Radiation in Moving Gaseous Media*, ed. Y. Chmielewski, & T. Lanz (Switzerland: Geneva Observatory), 337
- Frisch, H. 1996, *Sol. Phys.*, 164, 49
- Frisch, H. 2007, *A&A*, 476, 665
- Frisch, H., Anusha, L. S., Sampoorna, M., & Nagendra, K. N. 2009, *A&A*, 501, 335
- Gandorfer, A. 2000, *The Second Solar Spectrum, Vol. I: 4625 Å to 6995 Å* (Zurich: vdf Hochschulverlag)
- Gandorfer, A. 2002, *The Second Solar Spectrum, Vol. II: 3910 Å to 4630 Å* (Zurich: vdf Hochschulverlag)
- Gandorfer, A. 2005, *The Second Solar Spectrum, Vol. III: 3160 Å to 3915 Å* (Zurich: vdf Hochschulverlag)
- Hamilton, D. R. 1947, *ApJ*, 106, 457
- Heinzel, P. 1981, *J. Quant. Spec. Radiat. Transf.*, 25, 483
- Holzreuter, R., Fluri, D. M., & Stenflo, J. O. 2005, *A&A*, 434, 713
- Hubeny, I. 1982, *J. Quant. Spec. Radiat. Transf.*, 27, 593
- Hubeny, I. 1985a, *A&A*, 145, 463
- Hubeny, I. 1985b, in *Progress in Stellar Spectral Line*, ed. J. E. Beckman, & L. Crivellari (Dordrecht: Reidel), 27

- Hubeny, I., & Cooper, J. 1986, ApJ, 305, 852
- Hubeny, I., & Lites, B. W. 1995, ApJ, 455, 376
- Hubeny, I., Oxenius, J., & Simonneau, E. 1983a, J. Quant. Spec. Radiat. Transf., 29, 477
- Hubeny, I., Oxenius, J., & Simonneau, E. 1983b, J. Quant. Spec. Radiat. Transf., 29, 495
- Hummer, D. G. 1962, MNRAS, 125, 21
- Kneer, F. 1975, ApJ, 200, 367
- Landi Degl’Innocenti, E. 1983, Sol. Phys., 85, 3
- Landi Degl’Innocenti, E. 1984, Sol. Phys., 91, 1
- Landi Degl’Innocenti, E. 1998, Nature, 392, 256
- Landi Degl’Innocenti, E., Landi Degl’Innocenti, M., Landolfi, M. 1997, in Proc. Forum THÉMIS, Science with THÉMIS, ed. N. Mein & S. Sahal-Bréchet (Paris: Obs. Paris-Meudon), 59
- Landi Degl’Innocenti, E., & Landolfi, M. 2004, Polarization in Spectral Lines (Dordrecht: Kluwer)
- Manso Sainz, R., & Trujillo Bueno, J. 2003, Phys. Rev. Letters, 91, 111102
- Mihalas, D. 1978, Stellar Atmosphere (2nd ed.; San Francisco, CA: Freeman)
- Nagendra, K. N. 1994, ApJ, 432, 274
- Nagendra, K. N. 1995, MNRAS, 274, 523
- Nagendra, K. N., Frisch, H., & Faurobert, M. 2002, A&A, 395, 305
- Nagendra, K. N., Paletou, F., Frisch, H., & Faurobert-Scholl, M. 1999, in Solar Polarization, ed. K. N. Nagendra, & J. O. Stenflo (Boston: Kluwer), 127
- Nagendra, K. N., & Sampoorana, M. 2009, in ASP Conf. Ser. 405, Solar Polarization 5, ed. S. V. Berdyugina, K. N. Nagendra, & R. Ramelli (San Francisco: ASP), 261
- Omont, A., Smith, E. W., & Cooper, J. 1972, ApJ, 175, 185
- Omont, A., Smith, E. W., & Cooper, J. 1973, ApJ, 182, 283
- Rees, D. E., & Saliba, G. J. 1982, A&A, 115, 1

- Saliba, G. J. 1985, *Sol. Phys.*, 98, 1
- Saliba, G. J. 1986, PhD thesis, Univ. of Sidney
- Sampoorna, M., Nagendra, K. N., & Frisch, H. 2008b, *J. Quant. Spec. Radiat. Transf.*, 109, 2349
- Sampoorna, M., Nagendra, K. N., & Stenflo, J. O. 2007a, *ApJ*, 663, 625
- Sampoorna, M., Nagendra, K. N., & Stenflo, J. O. 2007b, *ApJ*, 670, 1485
- Sampoorna, M., Nagendra, K. N., & Stenflo, J. O. 2008a, *ApJ*, 679, 889
- Sampoorna, M., & Trujillo Bueno, J. 2010, *ApJ*, 712, 1331
- Stenflo, J. O. 1994, *Solar Magnetic Fields: Polarized Radiation Diagnostics* (Dordrecht: Kluwer)
- Stenflo, J. O. 2004, *Reviews in Modern Astronomy*, 17, 269
- Stenflo, J. O. 2006, in *ASP Conf. Ser. 358, Solar Polarization 4*, ed. R. Casini, & B. W. Lites (San Francisco, CA: ASP), 215
- Stenflo, J. O., & Keller, C. U. 1997, *A&A*, 321, 927
- Stenflo, J. O., & Stenholm, L. G. 1976, *A&A*, 46, 69
- Štěpán, J., & Trujillo Bueno, J. 2010, *ApJ*, 711, L133
- Trujillo Bueno, J. 1999, in *Solar Polarization*, ed. K. N. Nagendra, & J. O. Stenflo (Boston: Kluwer), 73
- Trujillo Bueno, J. 2001, in *ASP Conf. Ser. 236, Advanced Solar Polarimetry: Theory, Observations, and Instrumentation*, ed. M. Sigwarth (San Francisco, CA: ASP), 161
- Trujillo Bueno, J. 2003, in *ASP Conf. Ser. 288, Stellar Atmosphere Modeling*, ed. I. Hubeny, D. Mihalas, & K. Werner (San Francisco, CA: ASP), 551
- Trujillo Bueno, J. 2009, in *ASP Conf. Ser. 405, Solar Polarization 5*, ed. S. V. Berdyugina, K. N. Nagendra, & R. Ramelli (San Francisco, CA: ASP), 65
- Trujillo Bueno, J., Shchukina, N., & Asensio Ramos, A. 2004, *Nature*, 430, 326
- Uitenbroek, H. 2003, in *ASP Conf. Ser. 288, Stellar atmosphere modeling*, ed. I. Hubeny, D. Mihalas, & K. Werner (San Francisco: ASP), 597

Vernazza, J. E., Avrett, E. H., & Loeser, R. 1981, ApJS, 45, 635

Table 1. The height in the VALC model atmosphere at which lines of different strength  $r$  have  $\tau_{0\mu} = 1$ . Other model parameters are  $\lambda = 5000 \text{ \AA}$ ,  $\epsilon = 10^{-4}$ ,  $a = 10^{-3}$  and  $\Gamma_{\text{E}}/\Gamma_{\text{R}} = D^{(2)}/\Gamma_{\text{R}} = 0$ .

$r$	$z(\tau_{x\mu} = 1)$ in km $x = 0$ and $\mu = 0.11$	$z(\tau_{x\mu} = 1)$ in km $x = 0$ and $\mu = 1$
$2 \times 10^{-7}$	2148	1878
$2.5 \times 10^{-7}$	2118	1848
$3 \times 10^{-7}$	2088	1833
$4 \times 10^{-7}$	2058	1788
$5 \times 10^{-7}$	2028	1773
$10^{-6}$	1950	1680
$10^{-5}$	1670	1410
$10^{-4}$	1395	1125
$10^{-3}$	1120	855
$10^{-2}$	845	585
0.7	430	165

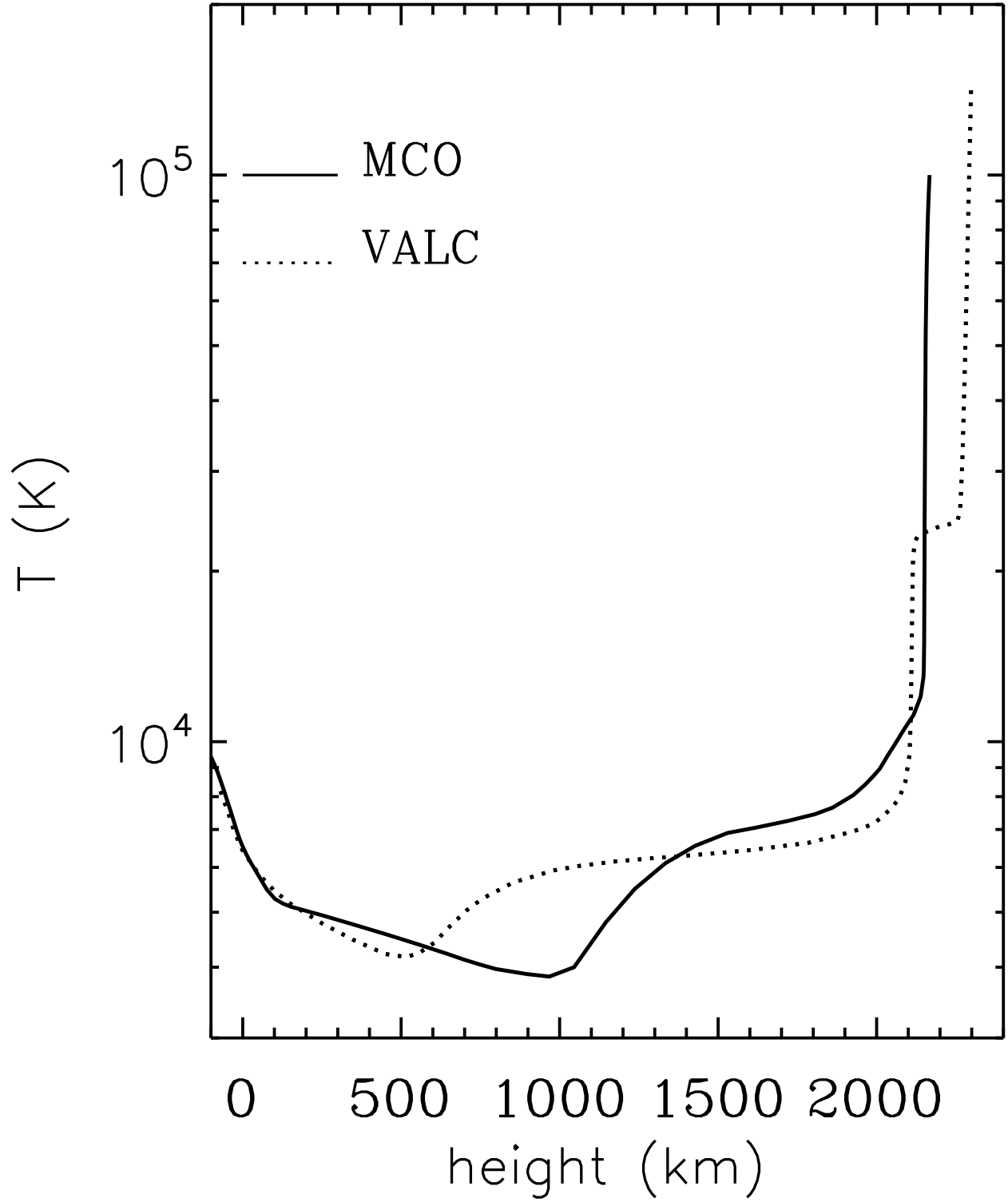


Fig. 1.— Temperature stratification of the VALC (dotted line) and MCO (solid line) solar model atmospheres. Note that between 600 and 1300 km (hereafter, the “lower chromosphere”) the MCO model is cooler than VALC.

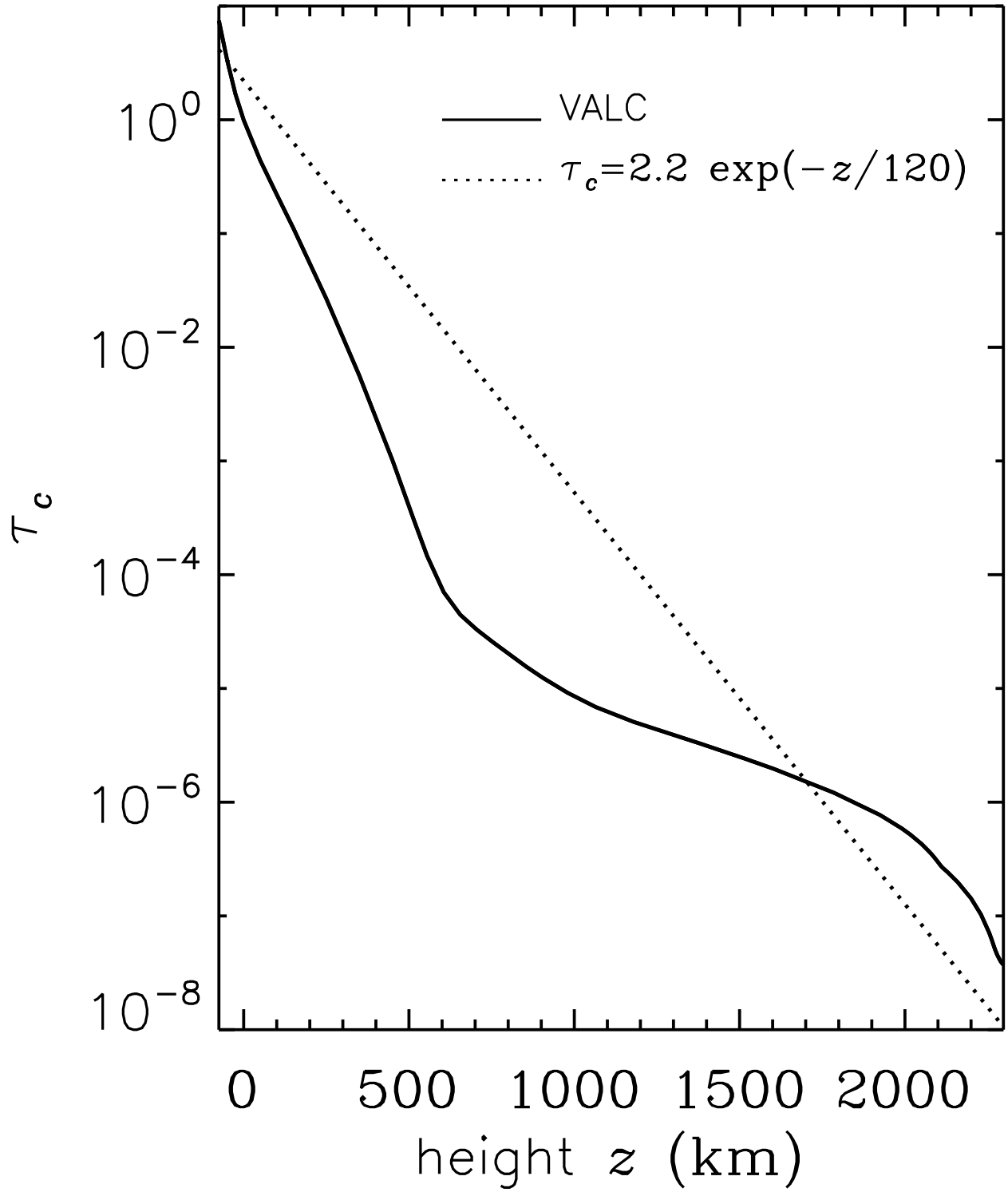


Fig. 2.— The continuum optical depth,  $\tau_c$  versus height in the VALC model atmosphere (solid line) and for a exponentially stratified atmosphere (dotted line). In this paper we have used  $\tau_c = 2.2 \exp(-z/H)$ , with  $H = 120$  km and  $z$  in km.



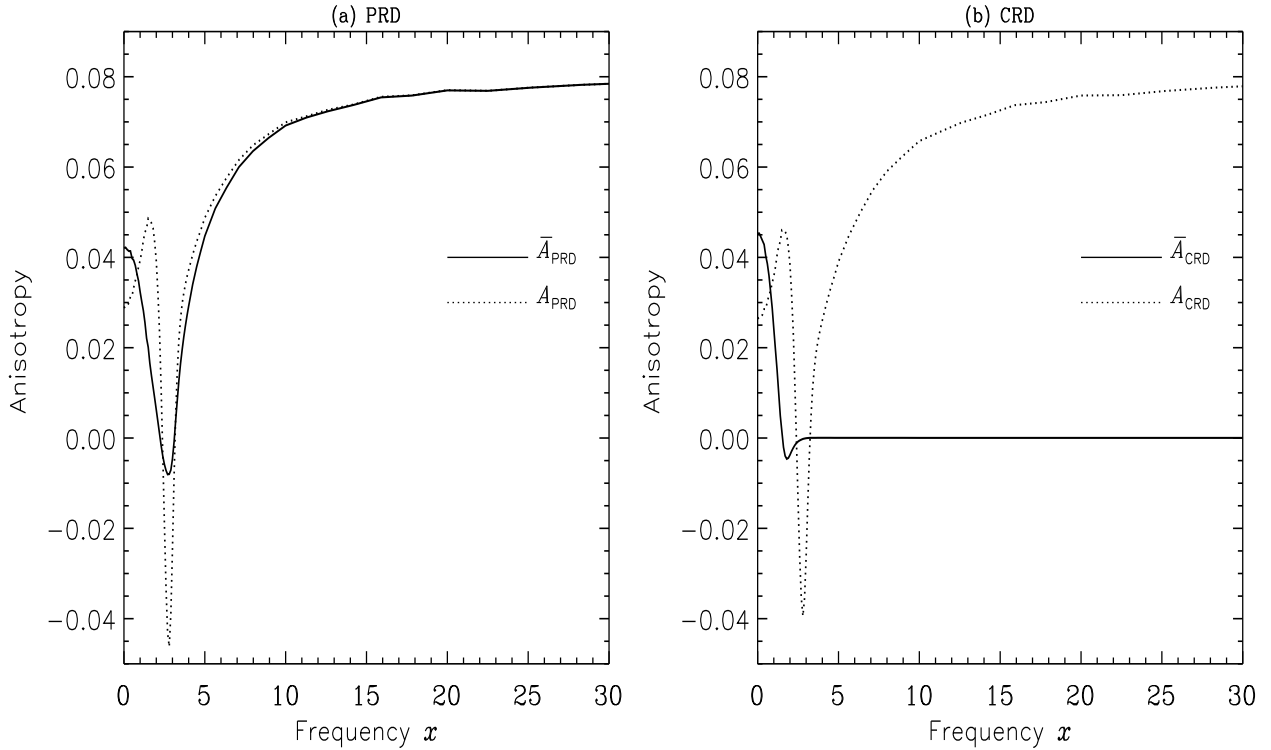


Fig. 3.— The anisotropy versus the reduced frequency  $x$  at the height in the VALC model atmosphere where  $\tau_{x\mu} = 1$  for a LOS with  $\mu = 0.11$ . Panels (a) and (b) correspond to PRD and CRD respectively. The other model parameters are  $\epsilon = 10^{-4}$ ,  $r = 10^{-5}$ ,  $a = 10^{-3}$  and  $\Gamma_E/\Gamma_R = D^{(2)}/\Gamma_R = 0$ . In both panels the solid line is  $\bar{A}$  and the dotted line is  $A$ . Notice that  $A_{\text{CRD}}$  and  $A_{\text{PRD}}$  are similar, while  $\bar{A}_{\text{CRD}}$  and  $\bar{A}_{\text{PRD}}$  differ greatly, particularly in the wings.

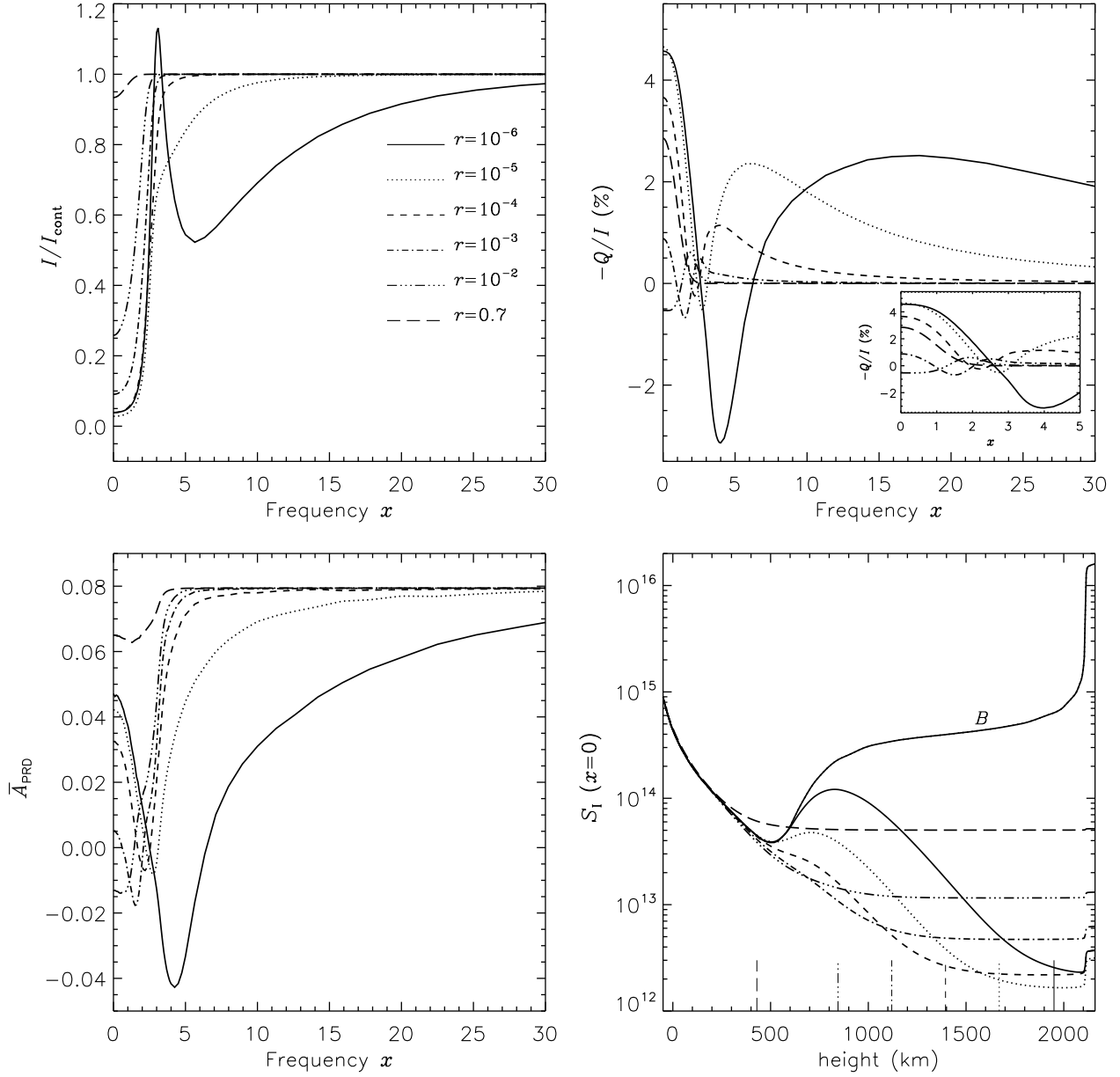


Fig. 4.— Sensitivity of the PRD solutions in the VALC model to the line strength parameter  $r$ . The different line types are the following. Solid:  $r = 10^{-6}$ ; dotted:  $r = 10^{-5}$ ; dashed:  $r = 10^{-4}$ ; dot-dashed:  $r = 10^{-3}$ ; dash-triple-dotted:  $r = 10^{-2}$ ; long-dashed lines:  $r = 0.7$ . Other model parameters are  $\lambda = 5000 \text{ \AA}$ ,  $\epsilon = 10^{-4}$ ,  $a = 10^{-3}$  and  $\Gamma_E/\Gamma_R = D^{(2)}/\Gamma_R = 0$ . The top solid line in the  $S_I$  panel is the Planck function  $B$  for the temperature stratification of the VALC model. The vertical lines in the same panel show the height at which  $\tau_{0\mu} = 1$  for a LOS with  $\mu = 0.11$ . The inset in the  $-Q/I$  panel shows the line core region in more detail. The symbol  $I_{\text{cont}}$  denotes the intensity at very large distance from line center.

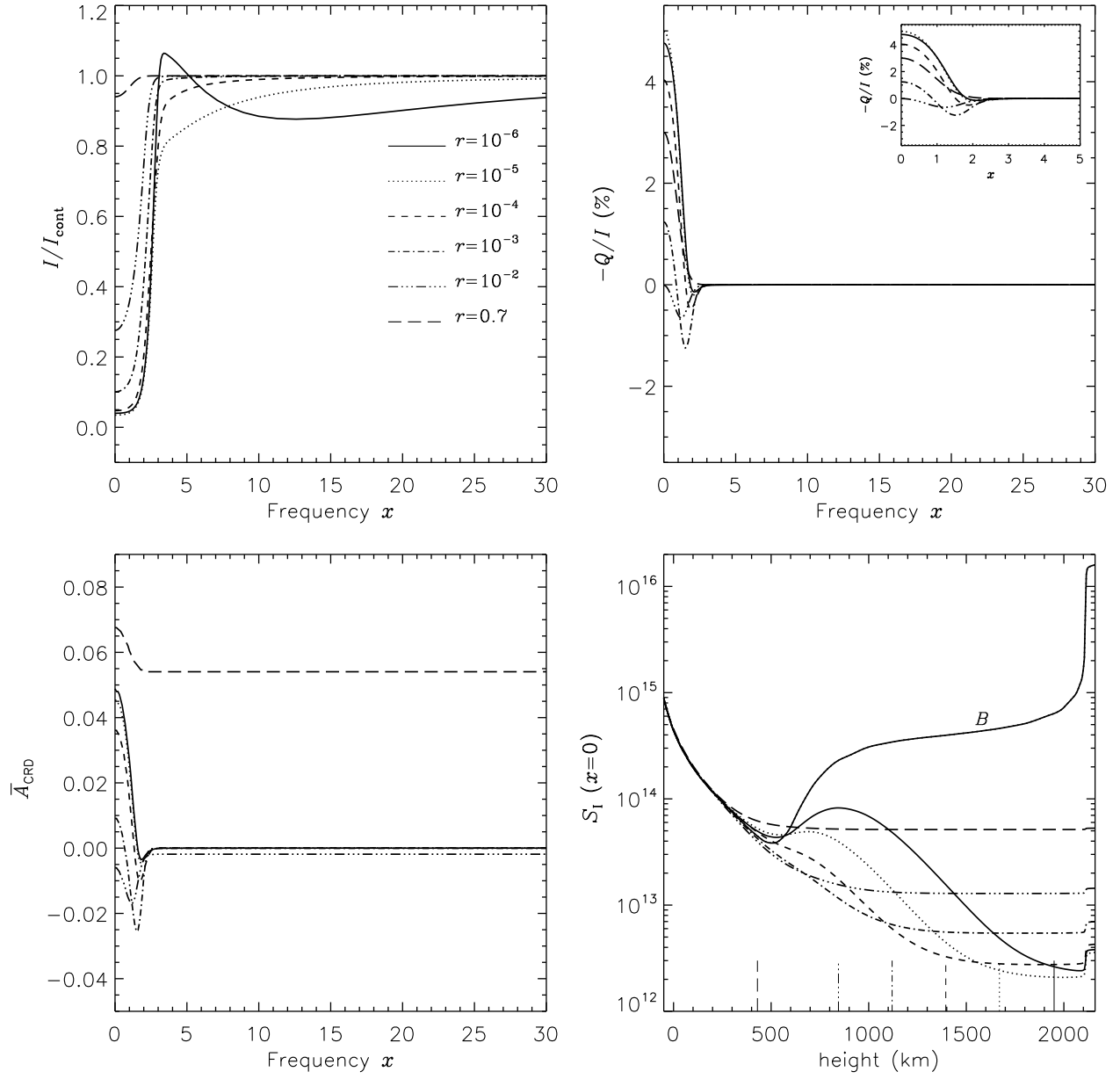


Fig. 5.— Same as Figure 4, but for CRD. The line types and the model parameters are exactly the same as in Figure 4.

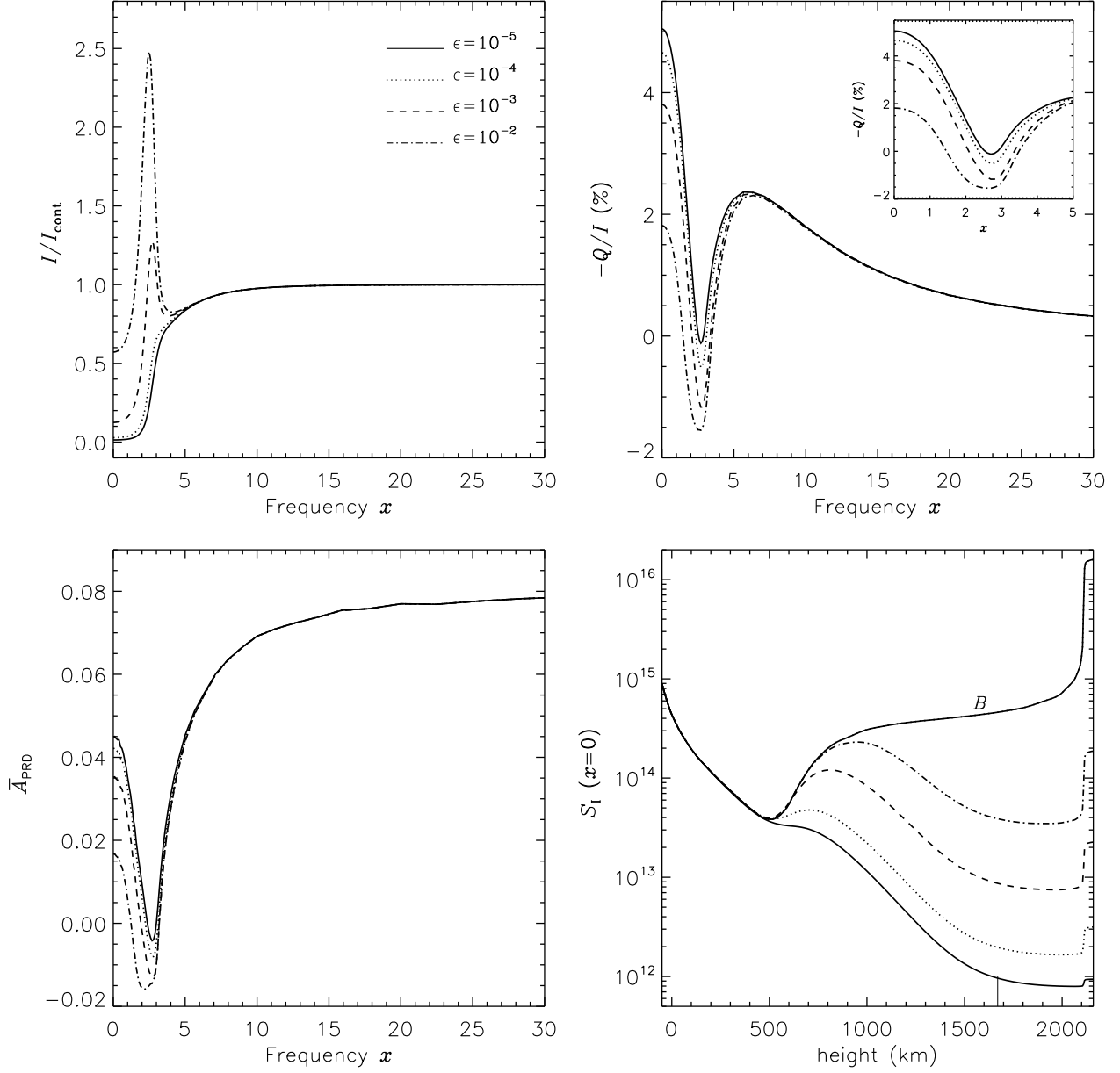


Fig. 6.— The effect of  $\epsilon$  on PRD solutions in the VALC model. The different line types are the following. Solid:  $\epsilon = 10^{-5}$ ; dotted:  $\epsilon = 10^{-4}$ ; dashed:  $\epsilon = 10^{-3}$ ; dot-dashed:  $\epsilon = 10^{-2}$ . Other model parameters are  $\lambda = 5000 \text{ \AA}$ ,  $r = 10^{-5}$ ,  $a = 10^{-3}$  and  $\Gamma_E/\Gamma_R = D^{(2)}/\Gamma_R = 0$ .

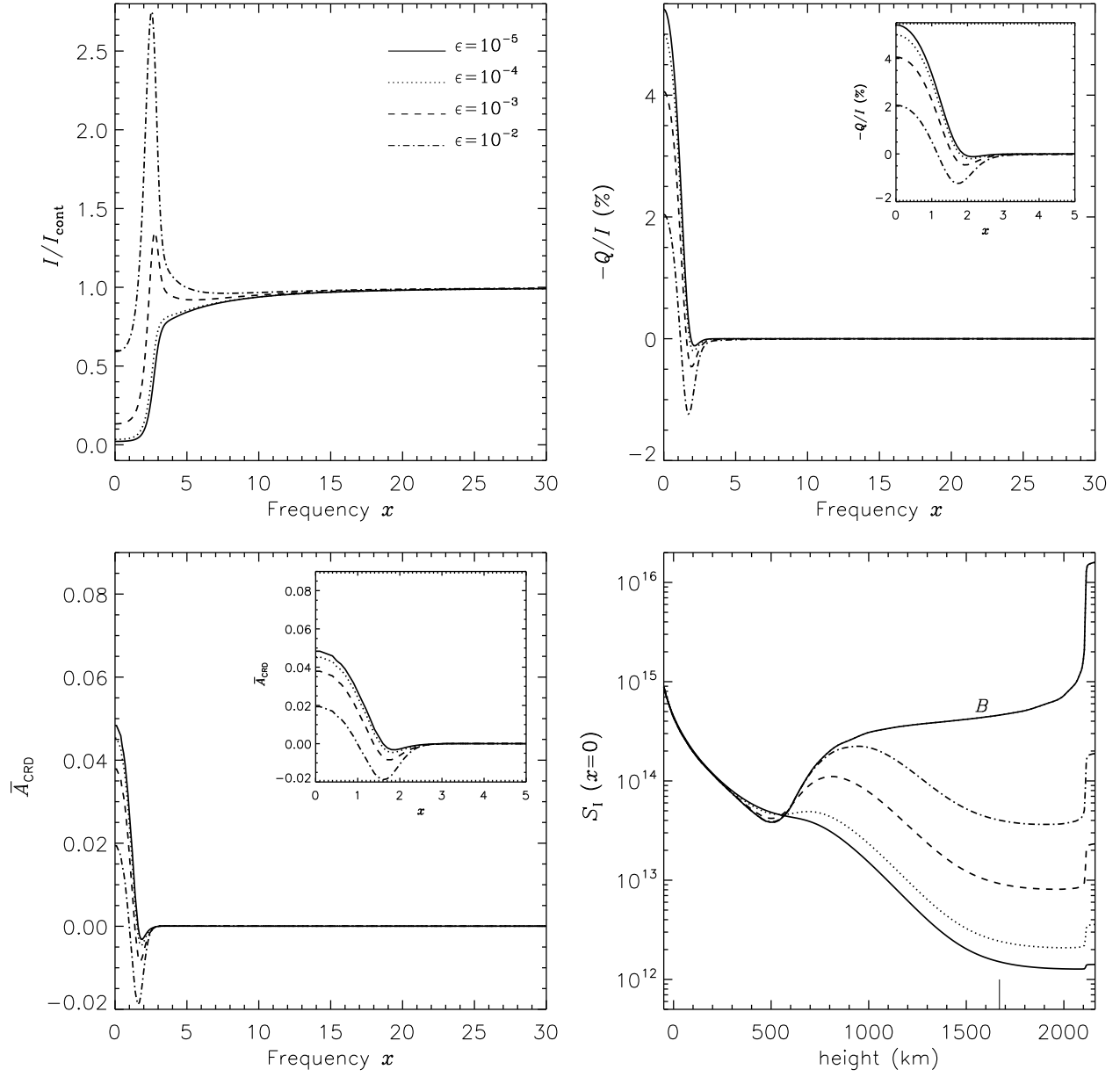


Fig. 7.— Same as Figure 6, but for CRD. The line types and the model parameters are exactly the same as in Figure 6.

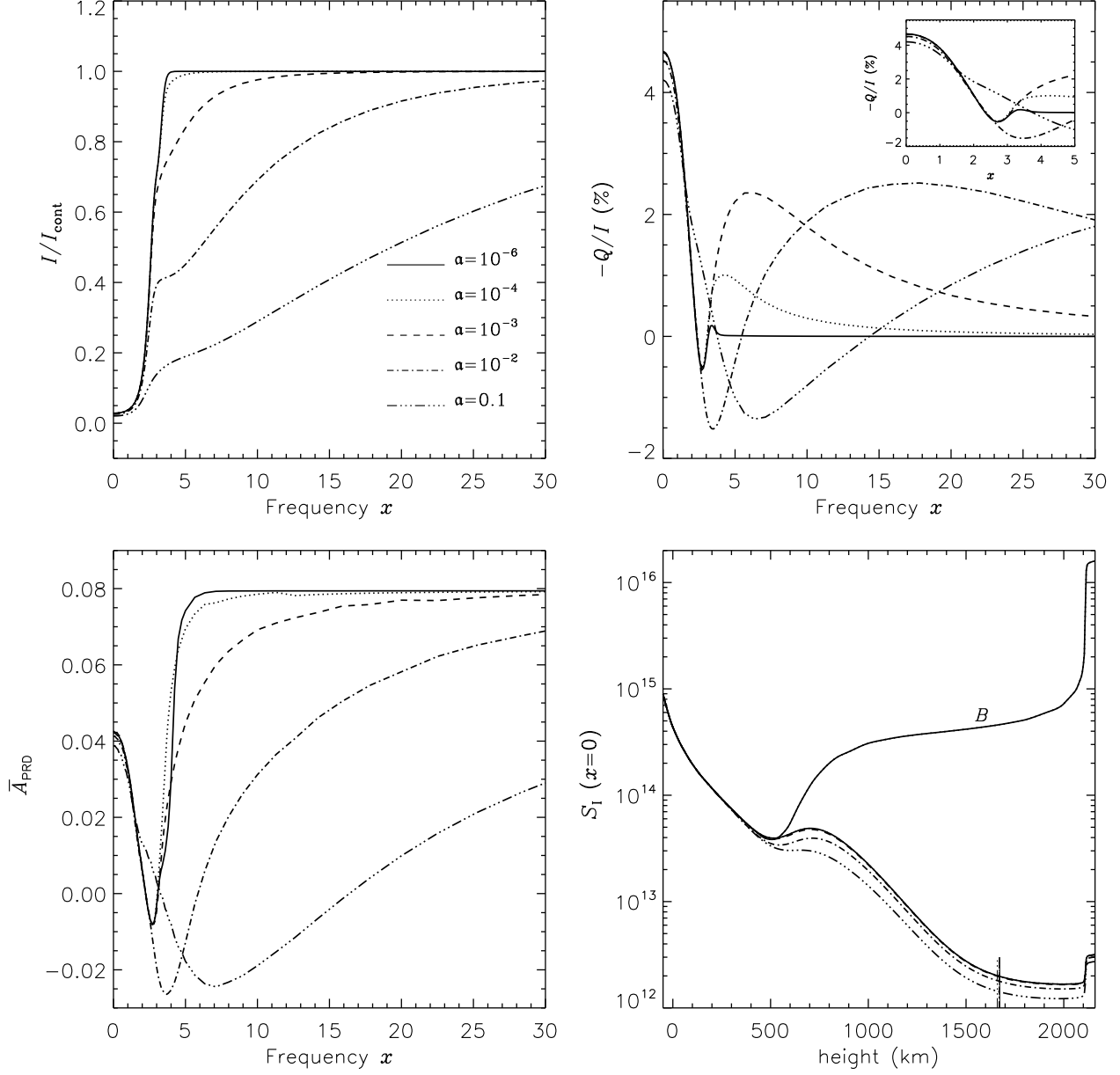


Fig. 8.— Sensitivity of the PRD solutions in the VALC model to variations in the damping parameter  $a$ . The different line types are the following. Solid:  $a = 10^{-6}$ ; dotted:  $a = 10^{-4}$ ; dashed:  $a = 10^{-3}$ ; dot-dashed:  $a = 10^{-2}$ ; dash-triple-dotted:  $a = 0.1$ . Other model parameters are  $\lambda = 5000 \text{ \AA}$ ,  $\epsilon = 10^{-4}$ ,  $r = 10^{-5}$ , and  $\Gamma_{\text{E}}/\Gamma_{\text{R}} = D^{(2)}/\Gamma_{\text{R}} = 0$ .

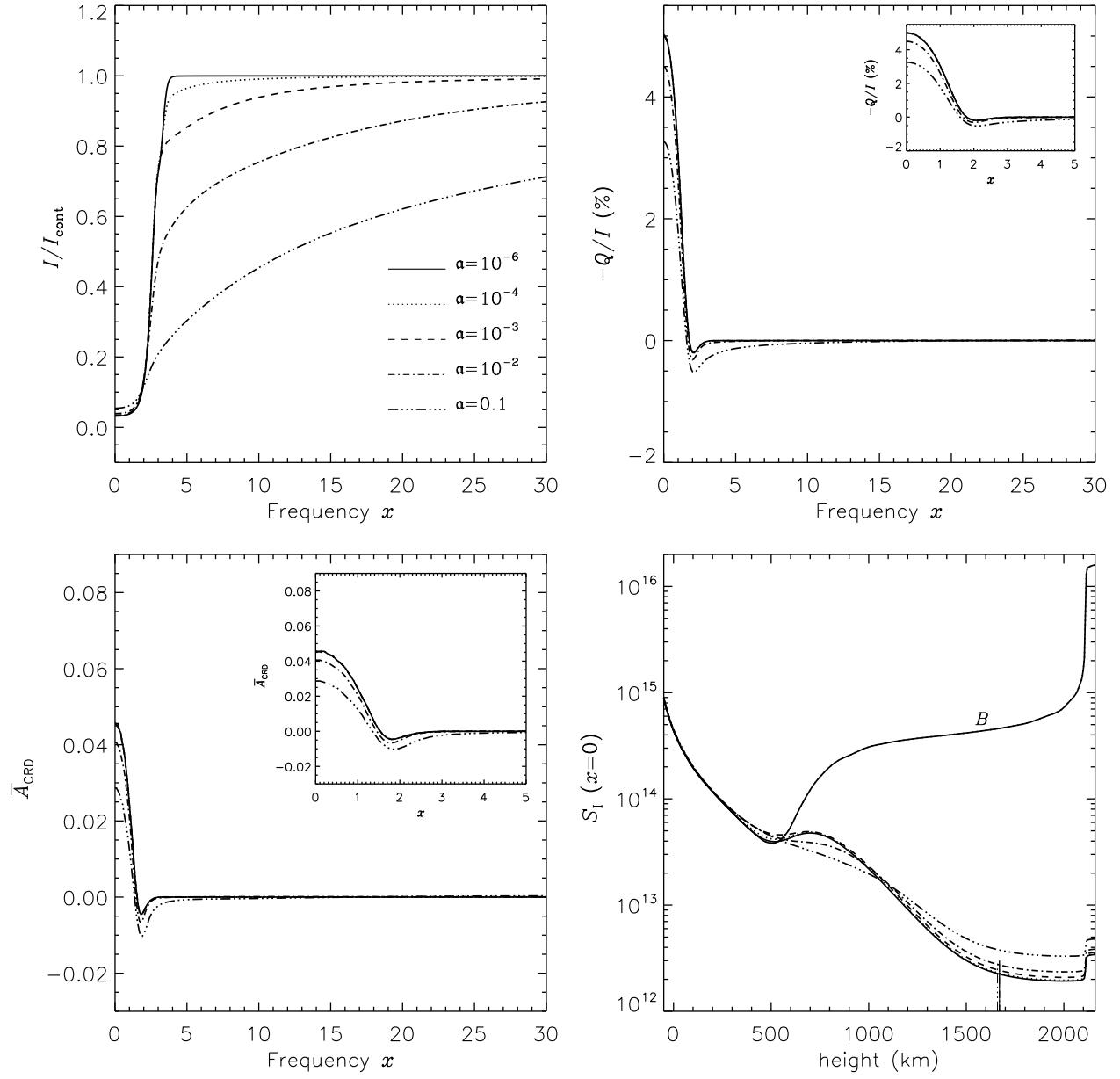


Fig. 9.— Same as Figure 8, but for CRD. The line types and the model parameters are exactly the same as in Figure 8.

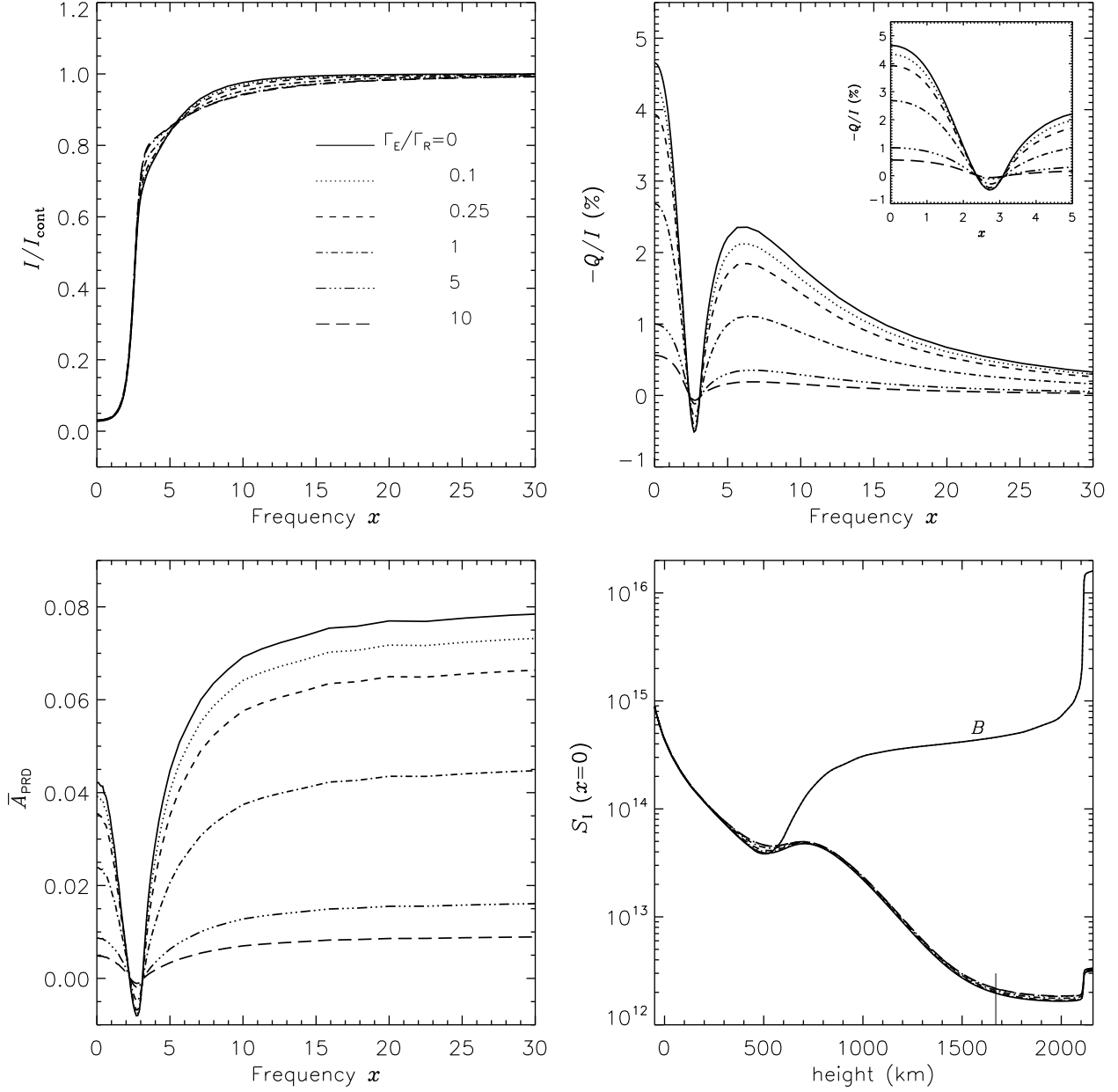


Fig. 10.— The effect of the elastic collisional rate  $\Gamma_E/\Gamma_R$  on the PRD solutions in the VALC model. The different line types are the following. Solid:  $\Gamma_E/\Gamma_R = 0$ ; dotted:  $\Gamma_E/\Gamma_R = 0.1$ ; dashed:  $\Gamma_E/\Gamma_R = 0.25$ ; dot-dashed:  $\Gamma_E/\Gamma_R = 1$ ; dash-triple-dotted:  $\Gamma_E/\Gamma_R = 5$ ; long-dashed:  $\Gamma_E/\Gamma_R = 10$ . Other model parameters are  $\lambda = 5000 \text{ \AA}$ ,  $\epsilon = 10^{-4}$ ,  $r = 10^{-5}$ ,  $a = 10^{-3}$  and  $D^{(2)}/\Gamma_R = 0.5 \Gamma_E/\Gamma_R$ .



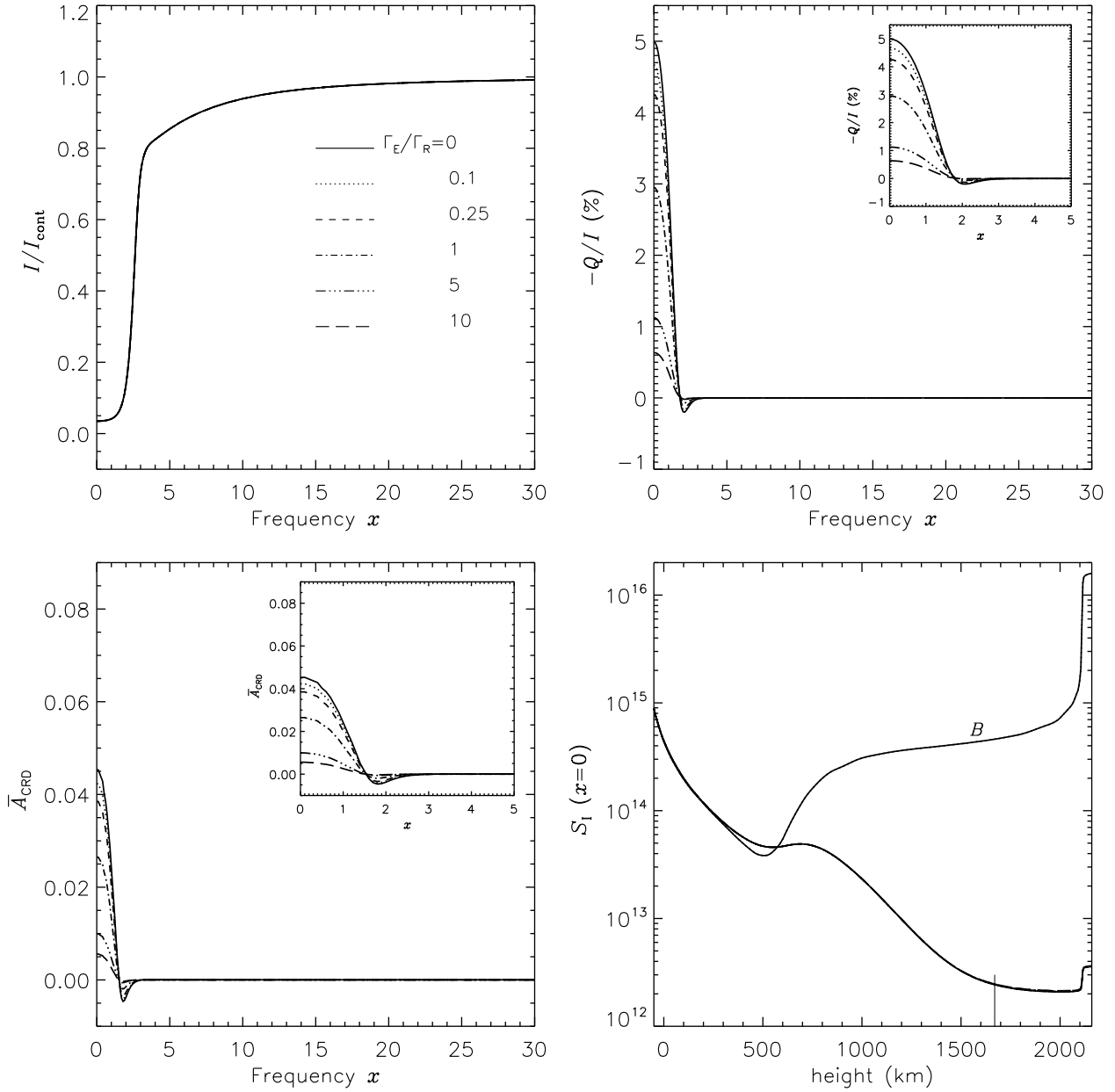


Fig. 11.— Same as Figure 10, but for CRD. The line types and the model parameters are exactly the same as in Figure 10.

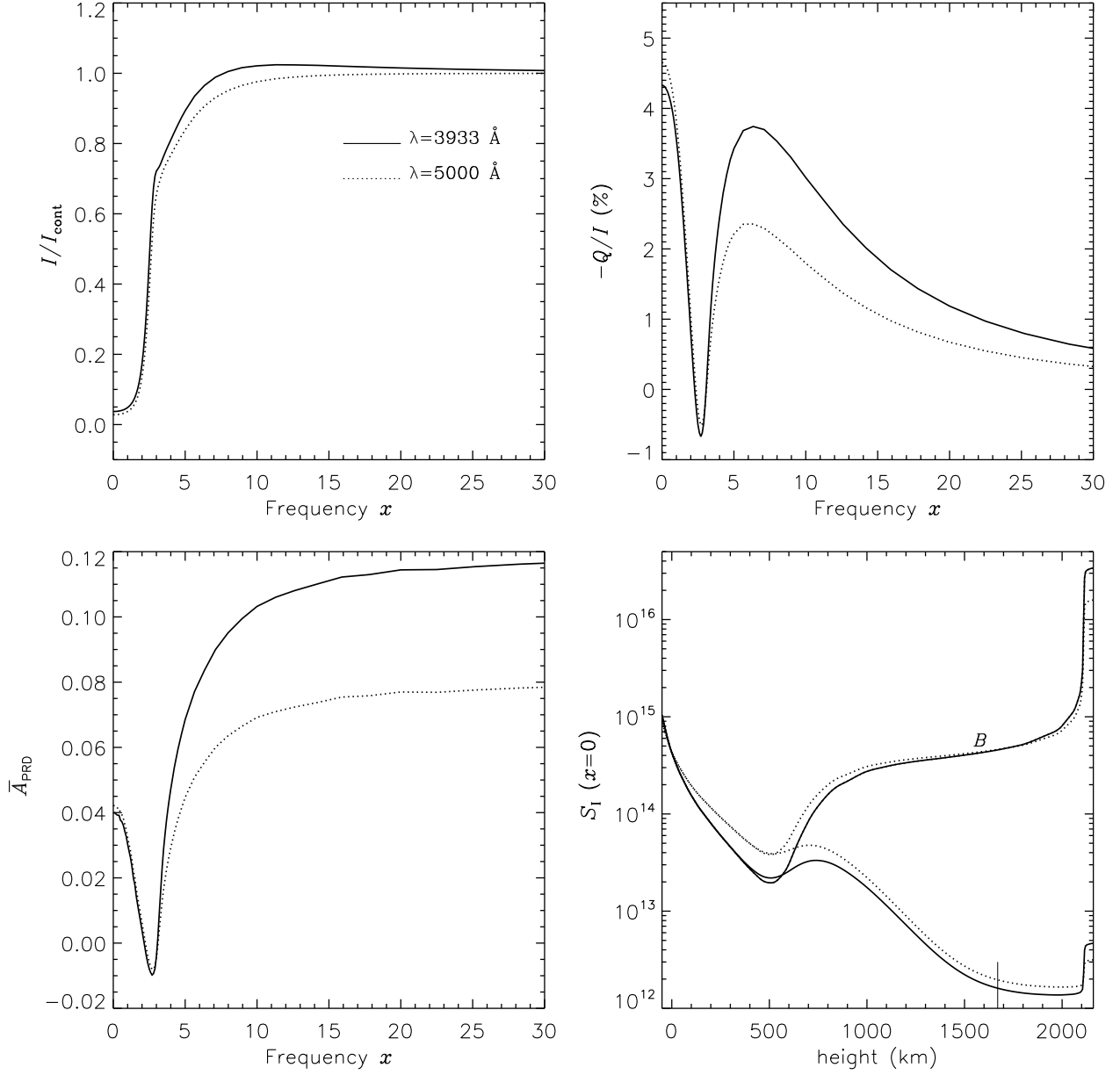


Fig. 12.— PRD solutions in the VALC model for two spectral lines with different wavelengths. Solid line:  $\lambda = 3933 \text{ \AA}$ ; dotted line:  $\lambda = 5000 \text{ \AA}$ . Other model parameters are  $\epsilon = 10^{-4}$ ,  $r = 10^{-5}$ ,  $a = 10^{-3}$  and  $\Gamma_E/\Gamma_R = D^{(2)}/\Gamma_R = 0$ .

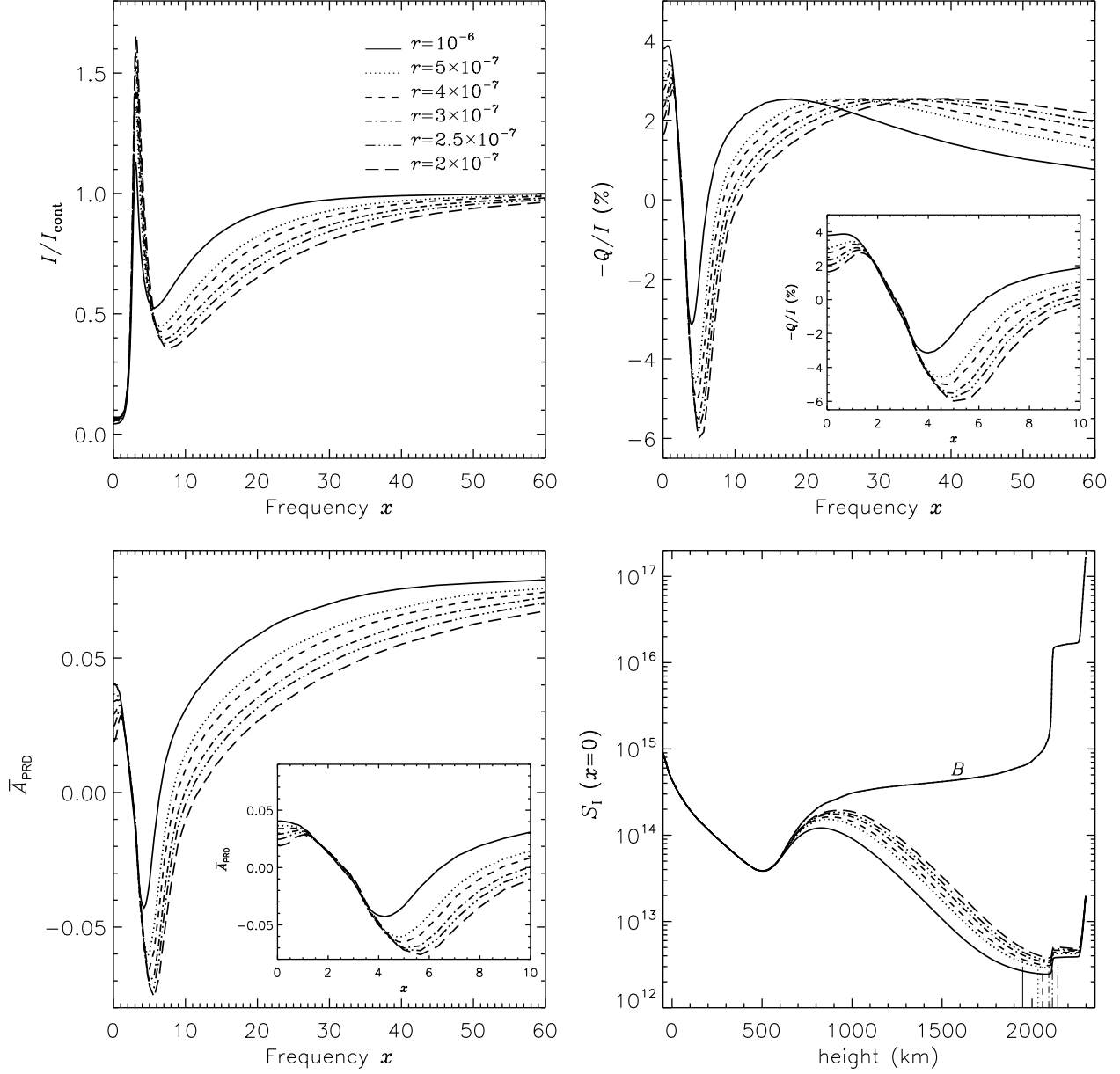


Fig. 13.— PRD solutions in the VALC model for spectral lines of the upper chromosphere and transition region. The different line types are the following. Solid:  $r = 10^{-6}$ ; dotted:  $r = 5 \times 10^{-7}$ ; dashed:  $r = 4 \times 10^{-7}$ ; dot-dashed:  $r = 3 \times 10^{-7}$ ; dash-triple-dotted:  $r = 2.5 \times 10^{-7}$ ; long-dashed lines:  $r = 2 \times 10^{-7}$ . Other model parameters are  $\lambda = 5000 \text{ \AA}$ ,  $\epsilon = 10^{-4}$ ,  $a = 10^{-3}$  and  $\Gamma_E/\Gamma_R = D^{(2)}/\Gamma_R = 0$ .

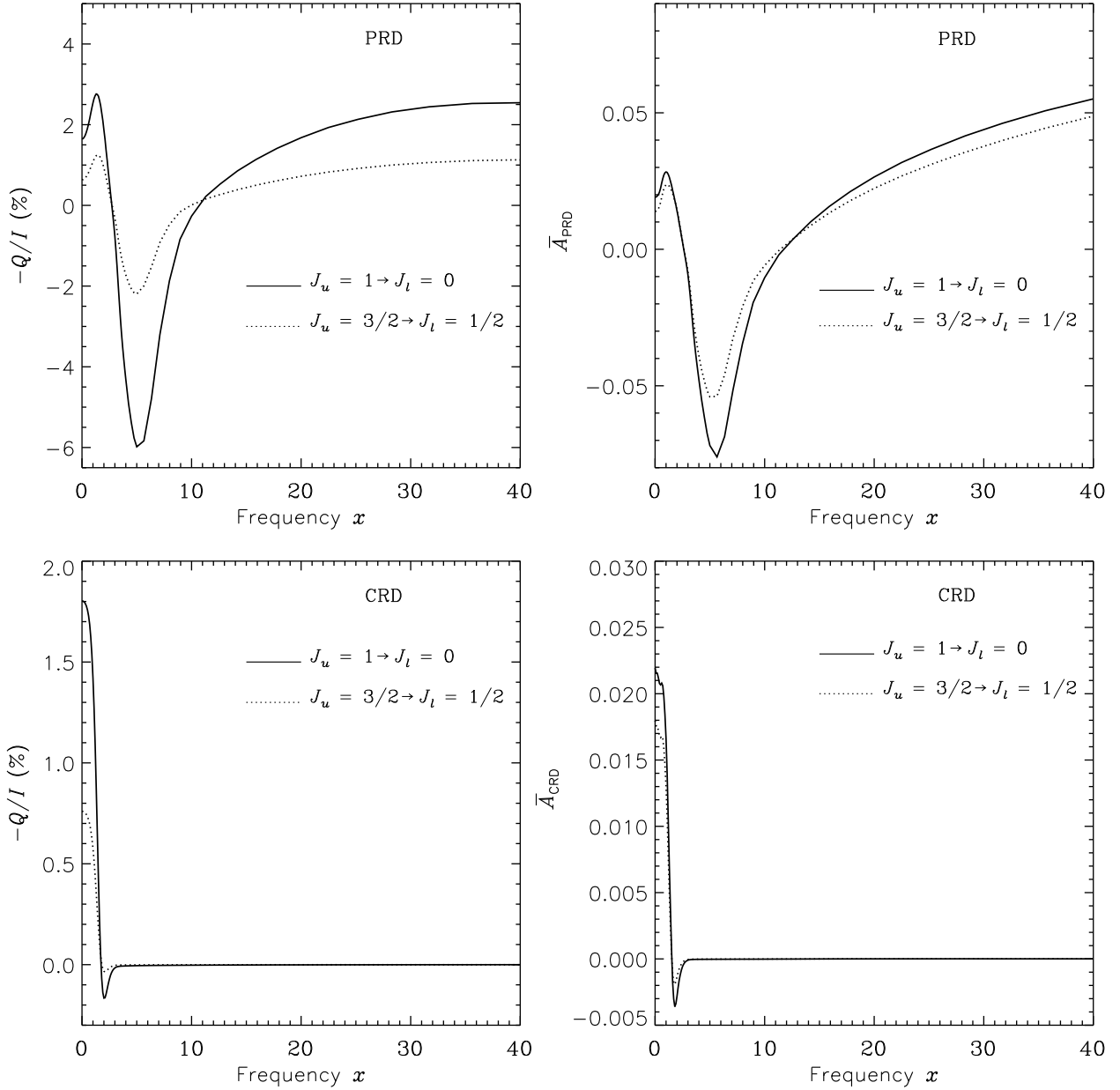


Fig. 14.— The effect of the  $W_2$  factor on the PRD (top panels) and CRD (bottom panels) solutions in the VALC model for a strong line with  $r = 2 \times 10^{-7}$ . Solid line:  $W_2 = 1$  (which corresponds to a line transition with  $J_l = 0$  and  $J_u = 1$ ); dotted line:  $W_2 = 0.5$  (which corresponds to a line transition with  $J_l = 1/2$  and  $J_u = 3/2$ ). Other model parameters are  $\lambda = 5000 \text{ \AA}$ ,  $\epsilon = 10^{-4}$ ,  $a = 10^{-3}$  and  $\Gamma_E/\Gamma_R = D^{(2)}/\Gamma_R = 0$ .

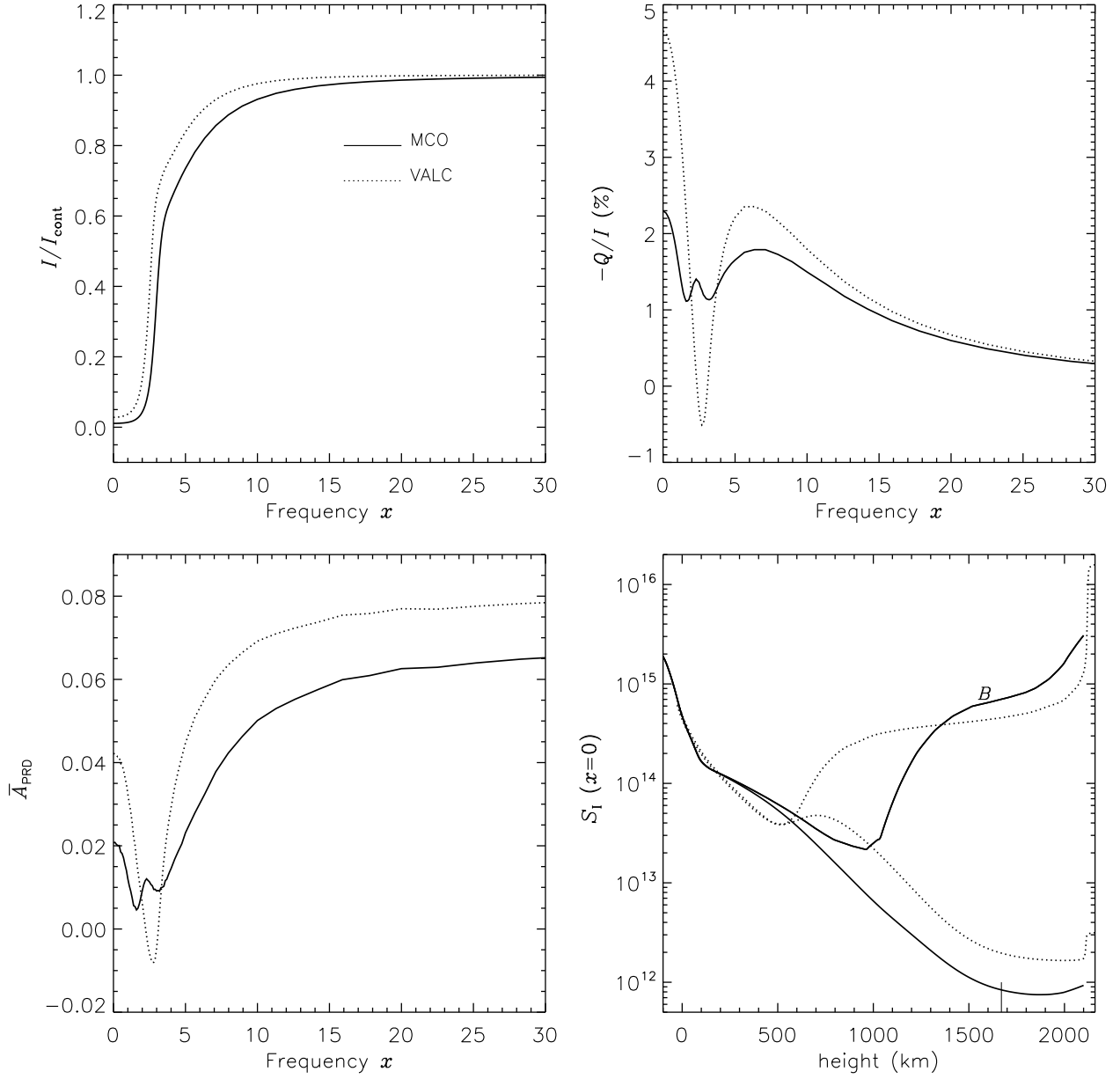


Fig. 15.— The effect of the atmospheric thermal structure on the PRD solutions. Solid lines: MCO model, dotted lines: VALC model. Other model parameters are  $\lambda = 5000 \text{ \AA}$ ,  $\epsilon = 10^{-4}$ ,  $r = 10^{-5}$ ,  $a = 10^{-3}$  and  $\Gamma_E/\Gamma_R = D^{(2)}/\Gamma_R = 0$ .

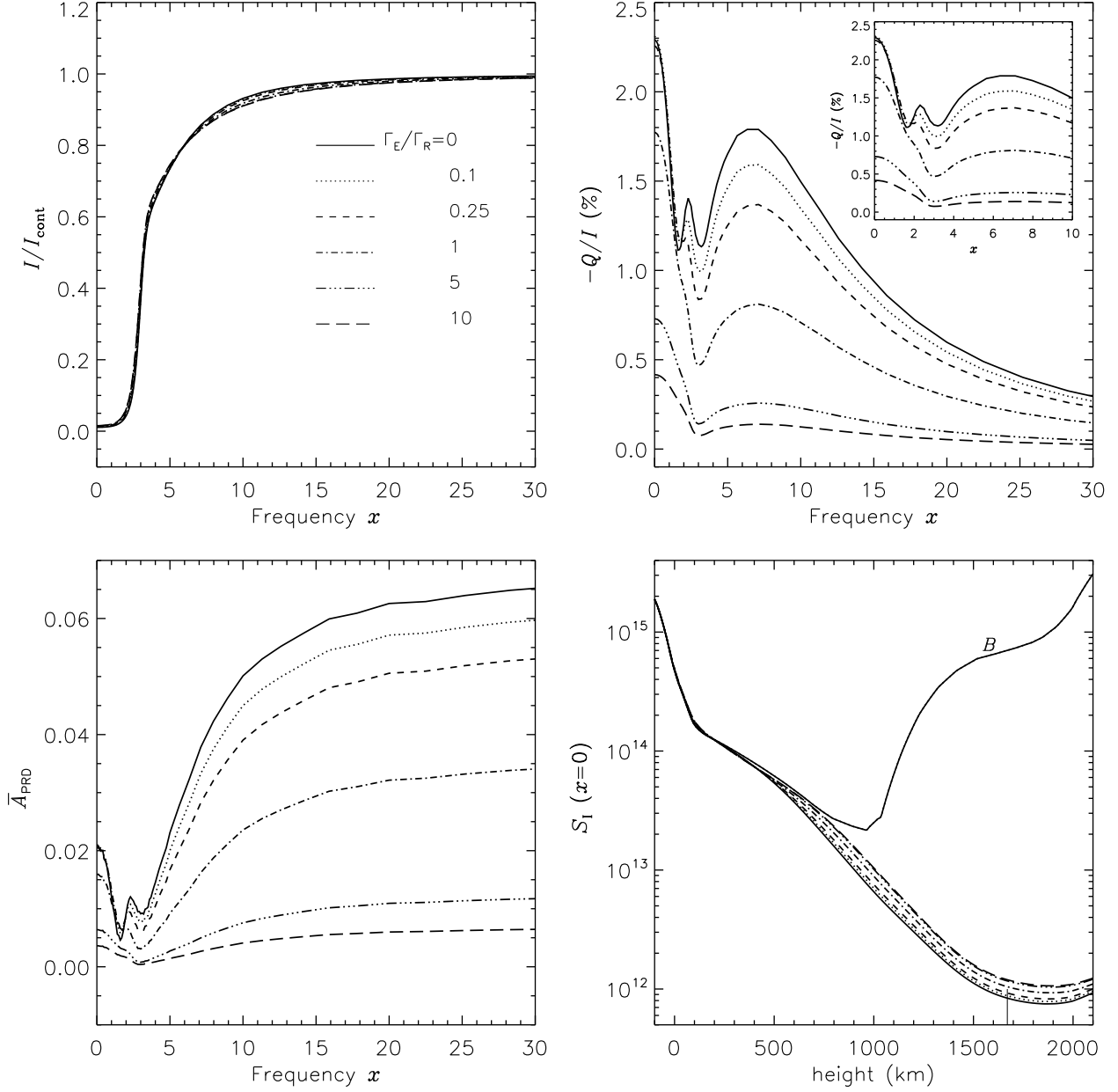


Fig. 16.— The effect of the elastic collisional rate  $\Gamma_E/\Gamma_R$  on the PRD solutions in the MCO model. The different line types are the following. Solid:  $\Gamma_E/\Gamma_R = 0$ ; dotted:  $\Gamma_E/\Gamma_R = 0.1$ ; dashed:  $\Gamma_E/\Gamma_R = 0.25$ ; dot-dashed:  $\Gamma_E/\Gamma_R = 1$ ; dash-triple-dotted:  $\Gamma_E/\Gamma_R = 5$ ; long-dashed lines:  $\Gamma_E/\Gamma_R = 10$ . Other model parameters are  $\lambda = 5000 \text{ \AA}$ ,  $\epsilon = 10^{-4}$ ,  $r = 10^{-5}$ ,  $a = 10^{-3}$  and  $D^{(2)}/\Gamma_R = 0.5 \Gamma_E/\Gamma_R$ .